Russian Chemical Reviews **81** (5) 458 – 475 (2012) © 2012 Russian Academy of Sciences and Turpion Ltd

DOI 10.1070/RC2012v081n05ABEH004251

Oxide ferromagnetic semiconductors: coatings and films

G D Nipan, A I Stognij, V A Ketsko

Contents

I.	Introduction	458
II.	Ion beam engineering of Co/TiO_2 multilayer nanostructure	459
III.	Solid solutions in the system Zn – Co – O	461
IV.	Search for DMS phases in the systems Mg – Ga(Al) – Fe – O	464
V.	Homogeneous complex metal – oxide films	469

Abstract. The review concerns the results of studies reported in the last decade and concerning oxide ferromagnetic semiconductors which retain the spin orientation of charge carriers above room temperature. Particular attention is paid to methods of preparation of diluted magnetic semiconductors. Methods of synthesis and peculiarities of the physicochemical properties of films and coatings based on ferromagnetic semiconductors are described and prospects for application of these compounds as materials for spintronics are discussed. The bibliography includes 160 references.

I. Introduction

The first ferromagnetic semiconductor (FS), europium monoxide, whose structure becomes magnetically ordered at $T < 77$ K, was discovered in 1961.[1] This discovery confirmed the feasibility of quantum magnetic recording where information is encoded through fixation of the spin orientation of charge carriers relative to the direction of external magnetic field.[2] However, the paramagnetic ($\Theta_C = 77$ K) (Ref. 1) and ferromagnetic [$T_C = 69.4$,[2] 66.8,[3,4] 69.15 K (Ref. 5)] Curie temperatures of EuO are low. This, as well as chemical degradation in air,[2] hampers technological applications of EuO single crystals or films.

Researchers working in the field of FS materials science pinned their hopes on the limited solid solutions of EuO with the samarium and ytterbium monoxides characterized by higher T_C: *e.g.*, T_C(SmO) = 130 K. However, further increase in the Curie temperature of solid solutions is limited by the limiting solubility of SmO in EuO (14 mol.%).[6] In addition, solid solutions $Eu_{1-x}Sm_xO$ or $Eu_{1-x}Yb_xO$ are chemically unstable similarly to EuO which exists only at low partial pressures of oxygen. A particular complicated problem consists in the nonstoichiometry of europium oxide with respect to oxygen, which significantly affects the properties of ferromagnetic semiconductors.

The discovery[6] in the mid-1960s of ferromagnetism in chalcogenide spinels of the general formula $A_{1\pm x}B_2C_{4\pm y}$ (A = Cd, Hg, Zn, Cu; B = Cr, Fe; C = S, Se, Te) and high T_C values (to 430 K) did not help to solve problems in FS materials science, namely, the compositions of nonstoichiometric phases $A_{1\pm x}B_2C_{4\pm y}$ including two volatile components are difficult to control during the growth of single crystals and films; similarly to the case of EuO, chemical degradation in air still remains of importance.

In 1996, a new type of 'hybrid' ferromagnetic semiconductors, $Ga_{1-x}Mn_xAs$ ($x < 5\%$) with $T_C = 170$ K, were prepared.[7] A characteristic feature of such phases is disordered distribution of magnetic impurity ions in the nonmagnetic crystal structure; therefore, they were called diluted magnetic semiconductors (DMS).

Progress in the field of DMS materials science led to theoretical studies[8,9] whose authors predicted that the orientation of the magnetic moments of ions, which is retained up to room temperature, can be obtained in wurtzite-type GaN and ZnO polymorphs doped with transition metal ions.

The idea to use an oxide semiconductor (or insulator) as matrix to dissolve the ferromagnetic oxide was checked experimentally. The results of studies carried out from 2000 to 2005 were generalized in reviews.[10–13] More recently, the search was focused on the preparation of DMS materials based on Co/ZnO and Co/TiO_2 nanostructures. The existence of ferromagnetism in homogeneous phases $Zn_{1-x}Co_xO$ ($x \leqslant 0.25$) is still a moot question.[14,15] Some authors reported the possibility of ferromagnetism in films,[16–25] nanowires[26–31] and $Zn_{1-x}Co_xO$ crystallites[32] to be observed up to room temperature (and above), whereas other authors report that the onset of ferromagnetism is observed upon annealing of samples *in vacuo*[33] or at low

G D Nipan, V A Ketsko N S Kurnakov Institute of General and Inorganic Chemistry, Russian Academy of Sciences, Leninsky prosp. 31, 119991 Moscow, Russian Federation. Fax (7-495) 954 12 79, tel. (7-495) 954 54 72, e-mail: nipan@igic.ras.ru (G D Nipan), tel. (7-495) 955 48 71, e-mail: ketsko@igic.ras.ru (V A Ketsko)
A I Stognij Scientific and Practical Materials Centre, National Academy of Sciences of Belarus, ul. P Brovki 19, 220072 Minsk, Republic Belarus. Fax/tel. (375-017) 284 13 06, e-mail: stognij@ifttp.bas-net.by

Received 6 July 2011
Uspekhi Khimii **81** (5) 458 – 475 (2012); translated by A M Raevskiy

partial pressures of oxygen,[34–36] in zinc vapours[33,37,38] or in inert atmosphere[39–41] and is associated with the formation of clusters of impurity phases,[37,38,42–44] the $Zn_{1-x}Co_xO$ solid solutions always being paramagnetic.[45–53] In the case of Co/TiO_2, one deals with doping[54–60] because the solubility of cobalt oxides in rutile or anatase is low and the onset of ferromagnetism cannot but associate with the formation of impurity phases. Moreover, the appearance of the magnetic response observed in studies of various materials can be due to the sensitivity of measuring devices, because 'instrumental illusion' of ferrimagnetic ordering in the structure of the semiconductor matrix may emerge even at a concentration ratio of the magnetic particles of the impurity phase to the nonmagnetic semiconductor (or insulator) of 1 : 2000.[61]

Two key research avenues in semiconductor materials science include:[62]

— studies on the composite structures comprising ferromagnetic materials and nonmagnetic semiconductors and

— investigations on homogeneous ferromagnetic semiconductors with $T_C > 300$ K.

Progress in both of them requires materials with reproducible properties. Uncontrolled distribution of impurities in the crystallites or clusters in thin films precludes the attainment of reproducibility. Meanwhile, most studies in the field of DMS materials science were carried out based on the potential of instrumental methods and without preliminary physicochemical analysis of the oxide systems, which assesses the thermodynamic compatibility of the semiconductor matrix and the ferromagnetic oxide. For instance, the complexity of preparation of a homogeneous DMS material based on TiO_2 in the system Co–Ti–O can be assessed by simply reading reference data on the Ti–O system.[63]

Titania has three polymorphs, namely, rutile, anatase and brookite. Rutile is stable, whereas the other two polymorphs are metastable; they are formed in the presence of impurities.[63] In addition, in the composition range $TiO_{1.7}$–$TiO_{1.9}$ there exists a homologous series of structurally similar phases of the general formula Ti_nO_{2n-1} ($n = 4–10$). The formation of a particular TiO_x phase is determined by the temperature and partial pressure of oxygen;[64] for instance, dissolution of CoO or Co_3O_4 in TiO_2 in the ternary system Co–Ti–O may lead to the formation of, *e.g.*, $CoTiO_3$.

Above 300 K, ferromagnetic ordering was observed in the anatase- or rutile-type $Ti_{1-x}Co_xO_2$ thin films ($x < 0.1$) prepared by different methods including pulsed laser deposition (PLD),[65–68] laser molecular beam epitaxy,[69,70] sputtering,[71] ion implantation[72] and decomposition of organometallic precursors.[73] In all cases, ferromagnetism can be explained by the presence of cobalt clusters. At the same time, if homogeneous $Ti_{1-x}Co_xO_2$ exhibits no properties of a ferromagnetic semiconductor, one can prepare a ferromagnetic semiconductor composite from thermodynamically compatible phases in the system Co–Ti–O. This problem was solved by fabricating a multilayer film.[74]

The authors of this review attempted to systematize the results of studies on oxide ferromagnetic semiconductors. The emphasis is placed on physicochemical analysis of DMS phases in the oxide systems, which allows one to predict the properties of films and coatings. Examples of DMS systems considered in the review were taken from the literature reported in the last decade and from the studies carried out by the authors of this review.

II. Ion beam engineering of Co/TiO_2 multilayer nanostructure

A specific feature of the spectroscopic dependences of the Faraday effect in the multilayer nanoscale Co/TiO_2 structure consists in the appearance of a resonance maximum, which depends on the number of pairs of layers.[75] A Co/TiO_2 structure formed on a GaAs substrate exhibited a giant injection magnetoresistance at room temperature.[76] The layer thicknesses at which the properties of these structures match those of bulk analogues were not optimized; however, the conditions for nucleation of cobalt films upon ion beam sputtering were established and the properties of such films that became increasingly thicker were compared with the properties of a bulk material. It was shown that (i) cobalt films thicker than 1.2 nm are continuous and their saturation magnetization is higher than that of bulk cobalt and (ii) the structural, electrical and nonmagnetic properties of the films thicker than 2 nm are similar to those of bulk specimens.[77,78] To create TiO_2 layers to 10 nm thick and multilayer Co/TiO_2 film nanostructures with a total thickness to 100 nm by ion beam sputtering deposition, a beam of 1.5-kEv argon ions with a current density of 0.25 mA cm^{-2} was used. Co/TiO_2 structures were formed by alternatively sputtering cobalt and titania. Films were deposited on silicon, gallium arsenide or quartz substrates, which were preliminarily exposed to ion beam finishing planarization of the surface to a root-mean-square roughness of less than 0.15 nm over a surface area to 6×6 μm^2 (Refs 79and 80). The electrical properties were analyzed using conventional two- and four-probe techniques.

It was found that TiO_2 films significantly change their optical properties in the thickness range from 2 to 10 nm. Figure 1 *a* presents the transmission spectra of layers of different thickness deposited on quartz substrates. As can be seen, no characteristic maxima in the region 380 nm are observed for the layers thicker than 6 nm and the net optical transparency of the layers is at most 80%. The transparency of the layers 2, 4, and 6 nm thick is higher than 90%; the transmission spectra of these layers exhibit local maxima in the short-wavelength spectral region, which can be compared with the transmission spectrum of anatase (curve *5*).[81] Taking into account these data, one can take it that under the chosen sputtering conditions, the TiO_2 films less than 6 nm thick have the anatase structure. The integrated transmission spectra of $[Co(2\text{ nm})/TiO_2(4\text{ nm})]_{15}$, $[Co(2\text{ nm})/TiO_2(2\text{ nm})]_{15}$ and $[Co(4\text{ nm})/TiO_2(4\text{ nm})]_{12}$ multilayer films are shown in Fig. 1 *b*. A comparison of the spectra presented in Fig. 1 *a*,*b* showed that at almost equal transparency of the TiO_2 layers 2 and 4 nm thick, the $[Co(2\text{ nm})/TiO_2(2\text{ nm})]_{15}$ structure is less transparent than $[Co(2\text{ nm})/TiO_2(4\text{ nm})]_{15}$, although they differ only in the total thickness of the TiO_2 layers.

Studies of the cross-sections of films revealed that if the cobalt and TiO_2 layers are less than 2 nm thick, they become indistinguishable as well as the interlayer boundaries.

This is probably due to mixing during the deposition of sputtered atoms with rather high energies. Under the experimental conditions in question, the path length of cobalt atoms (up to 1 nm) is comparable with the layer thickness ($\leqslant 2$ nm).[78] The mean free paths of titanium and oxygen atoms in the cobalt layer during the deposition estimated using the SRIM-2008 programme

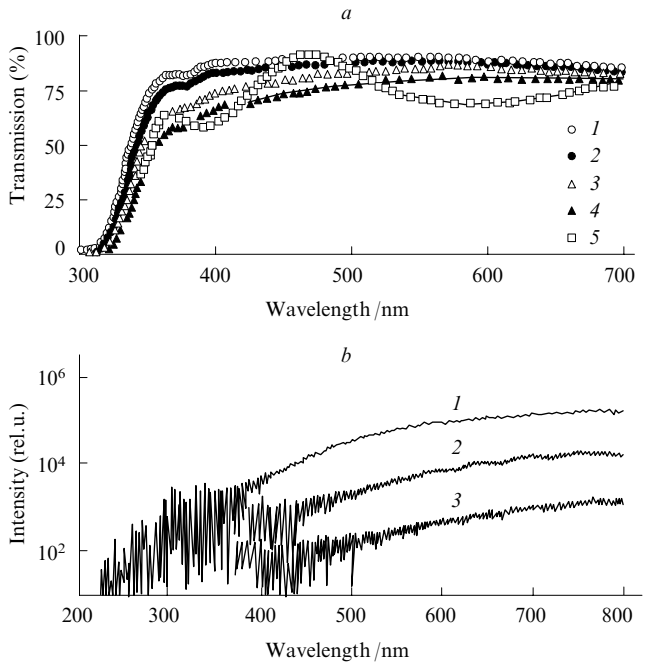


Figure 2. Cross-section of a multilayer film structure comprising Co and TiO_2 layers 4 nm thick (*a*) and the depth distribution profiles of cobalt (*1*), oxygen (*2*) and titanium atoms (*3*) in the Co(6 nm)/TiO_2(2 nm) multilayer structure (*b*).[78]

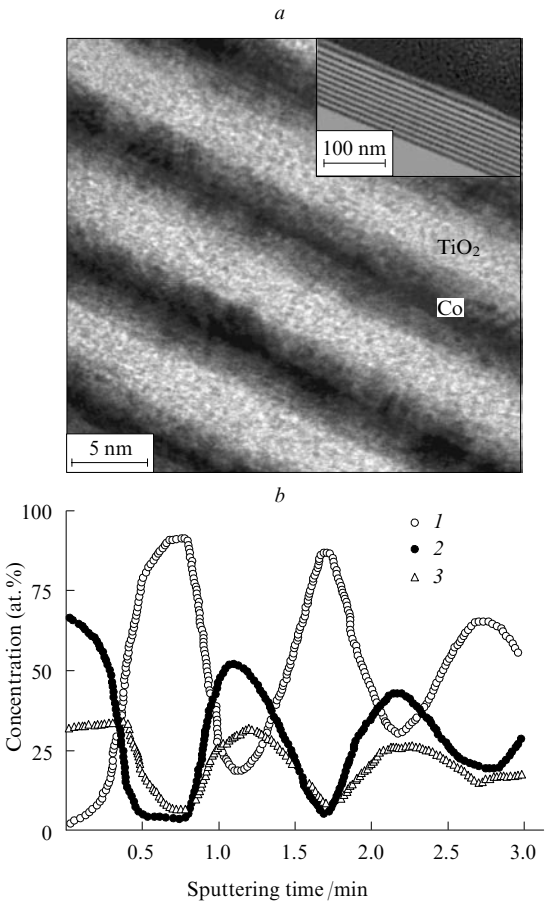


Figure 1. Transmission spectra of TiO_2 and anatase films (*a*) and multilayer film structures (*b*).[78]
(*a*) TiO_2 films 2 (*1*), 4 (*2*), 6 (*3*) and 10 nm thick (*4*); anatase film[81] 200 nm thick (*5*); (*b*) [Co(2 nm)/TiO_2(4 nm)]$_{15}$ (*1*), [Co(2 nm)/TiO_2(2 nm)]$_{15}$ (*2*) and [Co(4 nm)/TiO_2(4 nm)]$_{12}$ (*3*).

(http://www.srim.org/) also suggest the possibility of mixing of atoms in the course of retardation. Individual layers 2 to 4 nm thick become continuous and the interlayer boundaries become well-defined and plane-parallel, as can be seen in the cross-section of the structure formed by Co and TiO_2 layers (Fig. 2*a*).

Well-defined boundaries of layers 2 nm (and more) thick are confirmed by Auger spectroscopy data, but the escape depth of Auger electrons may reach a value of 2 nm,[82] which significantly reduces the possibility of layer separation. Taking into account this fact, a layer-by-layer analysis was performed by scanning with a 3-kEv argon ion beam. As a result, profiles of film structures with periodic coincidence of cobalt signal maxima with the titanium and oxygen signal minima for the number of pairs of layers of $\leqslant 10$ were obtained with good depth resolution. The characteristic depth profiles of the elements for the [Co(6 nm)/TiO_2(2 nm)]$_{12}$ film obtained for the first three pairs of layers is shown in Fig. 2*b*. As can be seen, a typical layered structure with clearly defined interfaces is formed in these cases even without correcting the experimental profiles in order to include the dynamic mixing effects in the layer-by-layer analysis and the finite escape depth of Auger electrons. Oxygen and titanium atoms are concentrated within the same regions. This to a first approximation allows one to exclude chemical interaction and the formation of Co–O and Co–Ti–O bonds near the boundaries. This conclusion is consistent with the known property of gettering of oxygen atoms by free titanium atoms.[83]

According to X-ray diffraction data, reflections from cobalt layers less than 4 nm thick are indiscernible against the noise level,[78] but the Co(100) and Co(002) reflections (hexagonal structure, space group $P6_3/mmc$) were observed for the Co/TiO_2 structures.

An analysis of the surface with an atomic force microscope (AFM) showed that, among all structures analyzed, only [Co(2 nm)/TiO_2(2 nm)]$_{15}$, [Co(2 nm)/TiO_2(4 nm)]$_{15}$ and [Co(4 nm)/TiO_2(4 nm)]$_{12}$ films were characterized by the root-mean-square roughness values smaller than 0.9 nm and had continuous surfaces (Fig. 3*a*). The surfaces of the [Co(4 nm)/TiO_2(2 nm)]$_{15}$ and [Co(6 nm)/TiO_2(2 nm)]$_{12}$ films were characterized by the root-mean-square roughness values from 1 to 2 nm and contained finite numbers of defects (surface pits). An AFM image of the surface of the [Co(4 nm)/TiO_2(2 nm)]$_{15}$ film with a surface pit density of $\sim 5 \times 10^7$ cm^{-2} is shown in Fig. 3*b*.

Measurements of electrical properties showed that the most transparent structure [Co(2 nm)/TiO_2(4 nm)]$_{15}$ was characterized by the highest surface resistance $\rho_s \approx 40$ Ω (square)$^{-1}$ and the multilayer structures [Co(2 nm)/TiO_2(2 nm)]$_{15}$ and [Co(4 nm)/TiO_2(2 nm)]$_{15}$ were characterized by $\rho_s \approx 12$ and 5 Ω (square)$^{-1}$, respectively.

The $I-V$ curves obtained using the conventional two-probe technique show a potential barrier of ~ 0.4 eV only for the best multilayer structure [Co(2 nm)/TiO_2(4 nm)]$_{15}$ formed on the Si(100) substrate and characterized by n-type conductivity and a specific resistance of 4.5 Ω cm. The potential barrier of 0.4 eV is comparable with the barrier determined for the structure Co/GaAs characterized by

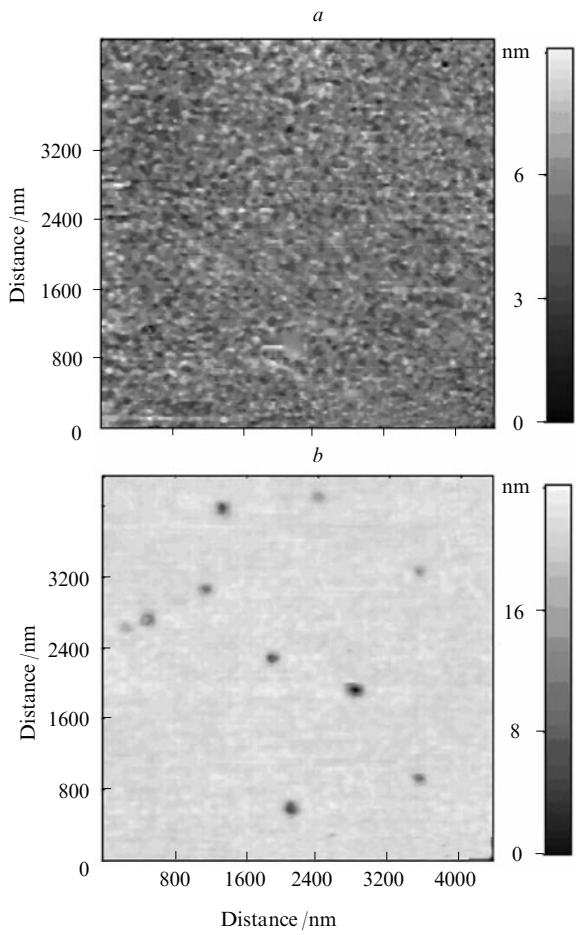


Figure 3. AFM images of the surface of multilayer film nanostructures $[Co(2\ nm)/TiO_2(2\ nm)]_{15}$ (*a*) and $[Co(4\ nm)/TiO_2(2\ nm)]_{15}$ (*b*).[78]

efficient room-temperature spin injection in the nonmagnetic semiconductor.[84]

The peculiarities of the engineering of continuous multilayer Co/TiO_2 nanostructures with clearly defined plane-parallel boundaries are due to both specific features of the ion beam sputtering deposition and the ability of nonstoichiometric titania in the nanostructured state to accumulate oxygen. The multilayer structures $[Co(2\ nm)/TiO_2(2\ nm)]_{15}$, $[Co(2\ nm)/TiO_2(4\ nm)]_{15}$ and $[Co(4\ nm)/TiO_2(4\ nm)]_{12}$ represent model systems for studies in magnetooptics and spintronics.

III. Solid solutions in the system Zn – Co – O

Zinc oxide films doped with transition metals from Cr to Cu using molecular beam epitaxy exhibit no ferromagnetic properties,[85] but some $Zn_{1-x}Co_xO$ films ($x = 0.05-0.25$) deposited on sapphire substrates by the PLD method appeared to be ferromagnetic and their Curie temperatures were higher than room temperature.[86]

Most transition metal oxides are poorly soluble in zinc oxide and replace at most 5% of the Zn^{2+} sites in the structure.[87] Therefore, considerable research efforts concerning $Zn_{1-x}Co_xO$ have been made and the results obtained appeared to be encouraging but ambiguous. Some authors reported the preparation of ferromagnetic ($T_C > 350$ K) homogeneous $Zn_{1-x}Co_xO$ films [$0 < x < 0.25$,[88] $x = 0.035-0.115$,[89] < 0.4,[90] 0.1 (Ref. 91)] containing no cobalt clusters by the sol–gel,[88] reactive sputtering[89,90] and PLD methods.[91] According to other authors,[92–94] wurtzite-type solid solutions $Zn_{1-x}Co_xO$ mainly show the properties of paramagnets, namely, ferromagnetic properties of the films ($x = 0.25$) obtained by the PLD method[92] appear only in the presence of cobalt clusters, whereas ferromagnetism in the polycrystals ($x = 0.05$, 0.1 and 0.15) synthesized by the solid-phase method[93] and in the melt-grown single crystals[94] is due to the presence of impurities. In some cases, information on the preparation of homogeneous ferromagnetic $Zn_{1-x}Co_xO$ films contradicts experimental data on the existence of 'alien' phases in these films.[95]

The 'alien' $Zn_yCo_{1-y}O$ ($y \leqslant 0.2$) and $Zn_zCo_{1-z}Co_2O_4$ ($z \leqslant 0.4$) phases, which are formed along with $Zn_{1-x}Co_xO$ in the system Zn – Co – O, represent solid solutions of ZnO in CoO[96,97] and Co_3O_4.[63] Crystalline oxides CoO (NaCl structural type) and Co_3O_4 (spinel structural type) undergo polymorphous transformations accompanied by antiferromagnetic ordering at 290 and 40 K, respectively.[63] Probably, these interrelated phenomena also occur in the solid solutions $Zn_yCo_{1-y}O$ and $Zn_zCo_{1-z}Co_2O_4$.

The phase states of the solid solutions $Zn_{1-x}Co_xO$ and $Zn_yCo_{1-y}O$ were studied more than four decades ago by Navrotsky and Muan[96,97] within the framework of investigations of the quasi-binary system ZnO – CoO. However, the quasi-binary approximation is not correct because the solid solutions $Zn_{1-x}Co_xO_{1+\delta}$, $Zn_yCo_{1-y}O_{1+\gamma}$ and $Zn_zCo_{1-z}Co_2O_{4+\varepsilon}$ (δ, γ and ε are the deviations from stoichiometry with respect to oxygen) in the ternary system Zn – Co – O were actually considered.

The content of oxygen in the crystalline phases based on CoO and Co_3O_4 is specified by the partial pressure of oxygen and varies within a few atomic per cent[98] and to a great extent determines the electrophysical properties of these oxides.[99] Even if we ignore the possibility of mutual clustering of solid solutions in the system Zn – Co – O and consider only homogeneous materials, the nonstoichiometry with respect to oxygen will strongly affect the semiconductor and magnetic properties of ternary crystals.

When comparing the magneto-electrical properties of $Zn_{1-x}Co_xO_{1+\delta}$ films[92] and polycrystals[93] formed under different conditions (873 K, 1.33×10^{-3} Pa and 1373 K, 20 kPa, respectively), one should keep in mind different relative content of oxygen $(1+\delta)$ in these systems.

To prepare crystalline phases with specified nonstoichiometry with respect to oxygen, one should preliminarily study the homogeneity regions of ternary solid solutions and to determine the temperature dependences of the partial pressure of oxygen for the δ-, γ- and ε-isoconcentrates in the quasi-binary approximation (at fixed zinc/cobalt content ratios). Having known these dependences, one can control the excess oxygen content in the solid solutions $Zn_{1-x}Co_xO_{1+\delta}$, $Zn_yCo_{1-y}O_{1+\gamma}$ and $Zn_zCo_{1-z}Co_2O_{4+\varepsilon}$. Taking into account the fact that crystals based on ZnO and CoO can undergo congruent sublimation,[64] oxygen deficiency in $Zn_{1-x}Co_xO_{1+\delta}$ and $Zn_yCo_{1-y}O_{1+\gamma}$ is very difficult to obtain. Vapours over oxygen-deficient ternary solid solutions mainly contain metals; the partial pressures of zinc, cobalt and cobalt oxide differ by a few orders of magnitude and are characterized by different temperature dependences.

In accordance with the function $P(T)$ for a monovariant equilibrium $CoO – Co_3O_4 – O_2$ the temperature of mutual

transformation of the oxides CoO and Co_3O_4 under isobaric condtions is determined by the external pressure. Initial data for studying the system Zn – Co – O can be obtained from the $P-T-x$ phase diagram of the system Co – O.[100] At an oxygen pressure of 100 kPa, the Co_3O_4-based crystalline phase exists to 1240 K; at $p_{O_2} \approx 21$ kPa, this temperature decreases to $\sim$1220 K.

Although ZnO crystallites have no effect on the activity of oxygen in the system Zn – Co – O, the vapour pressure over them can be rather high. Considering Zn – Co intermetallic compounds[101] at $T > 1240$ K in the absence of oxygen, there exist only a Co-based limited solid solution and a Zn-based melt. It should be noted that the solubility of zinc in crystalline cobalt at 1220 K can be as high as 30 at.%

To prepare homogeneous wurtzite-type $Zn_{1-x}Co_xO$ crystallites, phase equilibria involving solid solutions in the system Zn – Co – O were studied.[102] The character of magnetic ordering and the possibility of its variation upon

Table 1. Nominal and phase compositions of samples in the system Zn – Co – O.

Nominal composition	Phase composition	T/K	a/Å	c/Å
$Zn_{0.97}Co_{0.03}O$	ZnO + Co_3O_4	1073	–	–
	ssZnO	1173	3.238	5.183
$Zn_{0.95}Co_{0.05}O$	ZnO + Co_3O_4	1073	–	–
	ssZnO	1173	3.250	5.197
$Zn_{0.925}Co_{0.075}O$	ZnO + Co_3O_4	1073	–	–
	ssZnO + ssZnO (see [a])	1273	3.243	5.178
			3.252	5.197
	ssZnO	1373	3.247	5.192
$Zn_{0.9}Co_{0.1}O$	ZnO + Co_3O_4	1073	–	–
	ssZnO + ssCo_3O_4	1173	–	–
	ssZnO	1273	3.248	5.192
$Zn_{0.8}Co_{0.2}O$	ssZnO + ssCo_3O_4	1173	–	–
	ssZnO + ssCo_3O_4	1273	–	–
	ssZnO	1373	3.242	5.174
$Zn_{0.7}Co_{0.3}O$	ssZnO + ssCo_3O_4	1273	–	–
	ssZnO + ssCo_3O_4	1373	–	–
	ssZnO + ssCo_3O_4 + CoO	1423	–	–
$Zn_{0.6}Co_{0.4}O$	ssZnO + ssCo_3O_4	1423	–	–
$Zn_{0.2}Co_{0.8}O$	ssCoO	1423	4.237	–
$ZnCo_2O_4$	ZnO + ssCo_3O_4	1073	–	–
	ZnO + ssCo_3O_4	1173	–	–
	ssZnO + ssCo_3O_4	1273	–	–
	ssZnO + ssCo_3O_4	1373	–	–
	ssZnO + ssCo_3O_4 + CoO	1473	–	–
$(Zn_{0.9}Co_{0.1})Co_2O_4$	ZnO + ssCo_3O_4 + CoO	–	–	–
$(Zn_{0.6}Co_{0.4})Co_2O_4$	ZnO + Co_3O_4	1073	–	–
$Zn_{0.6}Co_{2.4}O_{4+\delta}$	ssCo_3O_4	1173	8.098	
	ssCo_3O_4 + CoO	1273	–	–
$(Zn_{0.3}Co_{0.7})Co_2O_4$	ZnO + Co_3O_4	1073	–	–
	ssCo_3O_4 + traces CoO	1173	8.085	–
$(Zn_{0.15}Co_{0.85})Co_2O_4$	ZnO + Co_3O_4	1073	–	–
	ssCo_3O_4 + traces CoO	1173	8.093	–
$Zn_{0.89}Co_{0.1}Eu_{0.01}O$	ssZnO + Eu_2O_3 (cubic)	1273	3.231	5.172
	ssZnO + Eu_2O_3 (cubic)	1373	3.244	5.180
	ssZnO + Eu_2O_3 (cubic)	1423	3.244	5.182
	ssZnO	1473	3.248	5.199
$Zn_{0.88}Co_{0.1}Eu_{0.02}O$	ssZnO + Eu_2O_3 (cubic)	1473	–	–
	ssZnO	1523	3.249	5.196
$Zn_{0.87}Co_{0.1}Eu_{0.03}O$	ssZnO	1523	–	–
$Zn_{0.85}Co_{0.1}Eu_{0.05}O$	ssZnO + Eu_2O_3 (monoclinic) + Eu_2O_3 (cubic)	1523	–	–
$Zn_{0.9}Co_{0.05}Eu_{0.05}O$	ssZnO + Eu_2O_3 (cubic)	1473		
$Zn_{0.89}Co_{0.1}Pr_{0.01}O$	ssZnO	1473	3.238	5.181
$Zn_{0.88}Co_{0.1}Sm_{0.02}O$	ssZnO + Sm_2O_3	1423	3.239	5.17
	ssZnO + ssZnO (see [a])	1473	3.232	5.16
			3.257	5.188
$Zn_{0.89}Co_{0.1}Nd_{0.01}O$	ssZnO + $NdCoO_3$	1473	–	–
	ssZnO	1523	3.252	5.184

[a] Two isostructural solid solutions were detected.

replacement of zinc ions by some other magnetic cations were established.

Polycrystalline samples were prepared by solid-phase synthesis from ZnO, Co_3O_4 and rare-earth element oxides or carbonates.

The chemical compositions (ignoring nonstoichiometry with respect to oxygen) and the phase compositions of polycrystals at different synthesis temperatures, as well as the lattice constants of homogeneous solid solutions $Zn_{1-x}Co_xO_{1\pm\delta}$ are listed in Table 1.

According to X-ray powder diffraction data, the solubility of CoO in the wurtzite-type ZnO matrix can be as high as 20 mol.% and the boundary compositions of the solid solutions vary with temperature. From the data of Table 1 it follows that all samples prepared at 1073 K (10 h annealing) contained two phases, *viz.*, ZnO and Co_3O_4. Noticeable solubility of cobalt oxides in ZnO is observed at $T > 1173$ K. At 1173 K, homogeneous samples of nominal chemical composition $Zn_{0.95}Co_{0.05}O$ can be prepared; at 1273 K, one gets $Zn_{0.9}Co_{0.1}O$ and at 1373 K, one deals with $Zn_{0.8}Co_{0.2}O$. Further heating causes decomposition of the solid solution and the appearance of the third phase based on CoO rather than an increase in the solubility of cobalt oxide.

Metastable clustering in wurtzite-type solid solutions $Zn_{1-x}Co_xO_{1+\delta}$, which are stable in the concentration range $0 \leqslant x \leqslant 0.2$ (see Table 1), was observed for the first time.

The temperature dependences of the heat capacity of the samples with the composition $Zn_{0.98}Co_{0.02}O$ (Ref. 103) and a mechanical mixture 0.98 ZnO + 0.02 CoO were studied in the range 5–350 K. A comparison showed no maximum at 288 K characteristic of CoO in the plot for $Zn_{0.98}Co_{0.02}O$. It was also shown that the heat capacity of $Zn_{0.98}Co_{0.02}O$ at $T > 80$ K is lower than that of the mechanical mixture 0.98 ZnO + 0.02 CoO, thus confirming the formation of the solid solution.

Based on the heat capacity data obtained at 290 K,[103] one can suggest that the CoO content in the solid solution sample studied was at most 0.3 mass %; this is consistent with the X-ray powder diffraction data.[102]

The temperature dependences of the magnetic susceptibility (Fig. 4) and specific magnetization (Fig. 5) of all solid solutions $Zn_{1-x}Co_xO$ were studied[102] by measuring the ponderomotive force in a magnetic field of 0.86 T in the range 77–700 K. The specific magnetization and magnetic susceptibility curves suggest the existence of two critical temperatures, $T_1 \approx 125$ K and $T_2 \approx 650$ K. One can assume that a magnetic order I – magnetic order II phase transition is observed at the temperature T_1 and a magnetic order II – magnetic disorder phase transition occurs at the temperature T_2. An analysis of the temperature dependences of σ and $1/\chi$ revealed a transition to the paramagnetic state at the temperature T_2.

In the temperature ranges 150–500 and 650–725 K, the magnetic susceptibility obeys the Curie–Weiss law. The Weiss temperatures are negative; this unambiguously gives the minus sign of the exchange coupling integral and suggests antiferromagnetic ordering of the solid solutions $Zn_{1-x}Co_xO_{1+\delta}$, which occurs until the Néel temperature (625 ± 25 K).

The observed anomalies in the temperature dependences of $1/\chi$ and σ in the temperature range studied may indicate changes not only in the magnetic ordering, but also in the crystal structure, *viz.*, probably, ZnO forms metastable

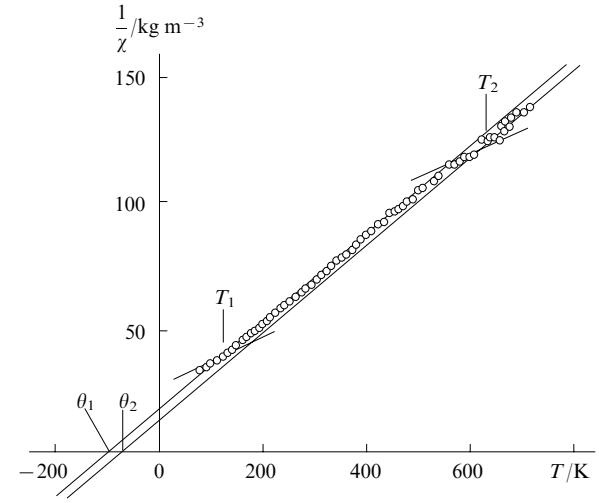


Figure 4. Temperature dependence of the inverse magnetic susceptibility ($1/\chi$) of the sample of nominal composition $Zn_{0.95}Co_{0.05}O$.[102]
θ_1 and θ_2 are the Weiss temperatures.

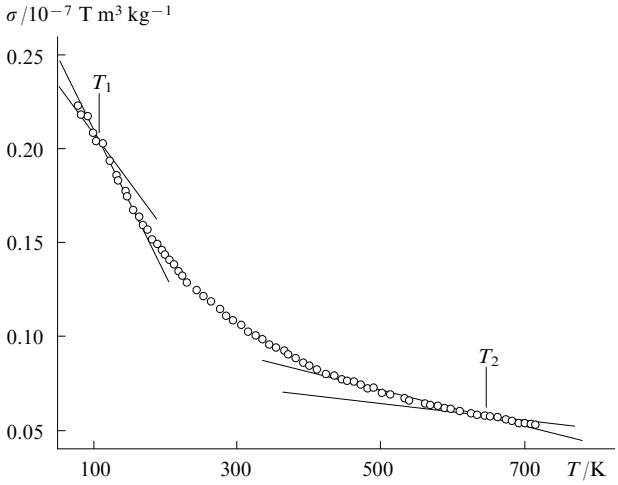


Figure 5. Temperature dependence of the specific magnetization (σ) of the sample of nominal composition $Zn_{0.95}Co_{0.05}O$.[102]

polymorphs with the NaCl and sphalerite (zinc blend) structural types.[11] In some cases, polymorphism of ZnO is due to the cubic structure of substrates or under the action of excess pressure;[11] it cannot be ruled out that the cobalt cations forming the cubic oxides CoO and Co_3O_4 can stabilize the systems.

Zinc oxide *per se* can stabilize the structures of cobalt oxides. At most 20% of cobalt cations can be replaced by zinc cations in the solid solutions $Zn_yCo_{1-y}O_{1\pm\gamma}$ and $Zn_yCo_{3-y}O_{4\pm\varepsilon}$ (see Table 1). Solid-phase synthesis is inappropriate for replacing cobalt atoms in the spinel structure of Co_3O_4 to obtain $ZnCo_2O_4$.[104]

Trace amounts of CoO observed in the $(Zn_{0.15}Co_{0.85})$. $.Co_2O_4$ and $(Zn_{0.30}Co_{0.70})Co_2O_4$ samples prepared at 1173 K at low zinc oxide concentrations disappear as the zinc oxide concentration increases. This unusual phenomenon can be explained using the phase diagram. Figure 6 presents the concentration diagram of the system

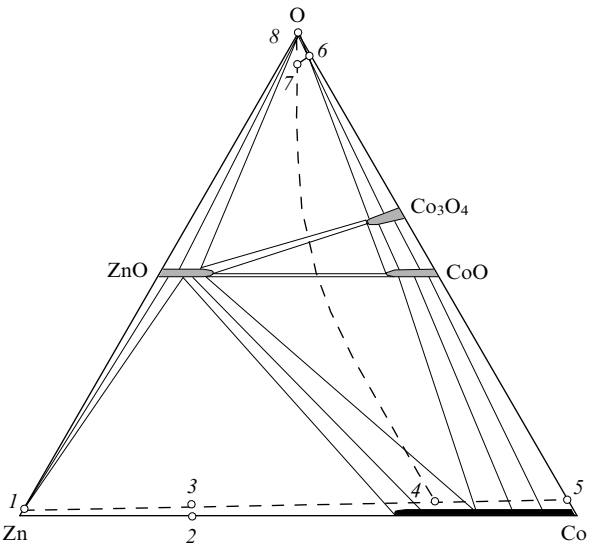


Figure 6. Concentration diagram of the system Zn – Co – O.[105]

Zn – Co – O.[105] The projection of the liquidus surface on the composition triangle is bounded by the dashed lines; the projection of the vapour surface is omitted for simplicity. The regions of solid solutions $Zn_{1-x}Co_xO_{1+\delta}$, $Zn_yCo_{1-y}O_{1+\gamma}$ and $Zn_zCo_{1-z}Co_2O_{4+\varepsilon}$ (given in grey) are interconnected by nodes, being also connected to the regions of crystalline cobalt (given in black), zinc vapours and oxygen.

Zigzag lines bound the projection of the crystallization surface: *1–3–4–7–8* for $Zn_{1-x}Co_xO_{1\pm\delta}$; *5–4–7–6* for $Zn_yCo_{1-y}O_{1\pm\gamma}$; *6–7–8* for $Zn_zCo_{3-z}O_{4\pm\varepsilon}$; *2–3–4–5* for the solid solution based on Co and *1–3–2* for the solid solution based on zinc. However, actual picture of phase equilibria involving solid solutions when using projections is more complicated.

Owing to the peritectic equilibrium $Zn_{1-x}Co_xO_{1\pm\delta}$ – $Zn_yCo_{1-y}O_{1\pm\gamma}$ – $Zn_zCo_{3-z}O_{4\pm\varepsilon}$ – melt (point *7* in Fig. 6) the solid solution based on Co_3O_4 in the ternary system can exist at higher temperatures than pure Co_3O_4.

Four univariant four-phase equilibria involving $Zn_{1-x}Co_xO_{1+\delta}$ and vapour (see Fig. 6) occur in the system:

$Zn_{1-x}Co_xO_{1+\delta}$ – Co – Zn-based melt – Zn vapour;

$Zn_{1-x}Co_xO_{1+\delta}$ – Co – $Zn_yCo_{1-y}O_{1+\gamma}$ – O_2;

$Zn_{1-x}Co_xO_{1+\delta}$ – $Zn_yCo_{1-y}O_{1+\gamma}$ – $Zn_zCo_{1-z}Co_2O_{4+\varepsilon}$ – O_2;

$Zn_{1-x}Co_xO_{1+\delta}$ – $Zn_zCo_{1-z}Co_2O_{4+\varepsilon}$ – oxygen saturated melt – O_2.

The last-mentioned equilibrium is hypothetical because above 1243 K Co_3O_4 completely dissociates at atmospheric pressure of oxygen [64] without reaching incongruent melting. Therefore, an univariant equilibrium

$$Zn_{1-x}Co_xO_{1+\delta} - Zn_yCo_{1-y}O_{1+\gamma} - \text{melt} - O_2$$

is more probable.

The compositions of crystalline solid solutions $Zn_{1-x}Co_xO_{1+\delta}$, $Zn_yCo_{1-y}O_{1+\gamma}$ and $Zn_zCo_{1-z}Co_2O_{4+\varepsilon}$ vary with temperature and pressure.

Control of the properties of solid solutions $Zn_{1-x}Co_xO_{1+\delta}$ by varying the δ value is almost unsolvable task. Yet another method is to introduce one more magnetic ion into wurtzite structure of $Zn_{1-x}Co_xO_{1+\delta}$. Since iron and nickel occupy less than 1% of Zn^{2+} sites in such a solid-phase solution and homogeneous polycrystals of nominal composition $Zn_{0.89}Co_{0.10}Fe(Ni)_{0.01}O$ are not formed, lanthanide oxides were chosen for systematic studies.[102]

Quaternary ceramics were prepared by solid-phase synthesis. It was found that oxides of four lanthanides (Pr, Nd, Sm and Eu) can form limited solid solutions with $Zn_{0.9}Co_{0.1}O_{1+\delta}$ (see Table 1).

Studies of the magnetic properties showed that the introduction of the third cation did not lead to violation of antiferromagnetic ordering in the wurtzite structure of the ZnO matrix, but investigation of the lanthanide-doped samples confirmed the possibility of structural disordering in solid solutions $Zn_{1-x}Co_xO_{1+\delta}$, *viz.*, splitting of reflections in the X-ray diffraction patterns found for $Zn_{0.925}Co_{0.075}O_{1+\delta}$ was also observed in the X-ray diffraction patterns of the solid solution $Zn_{0.88}Co_{0.10}Sm_{0.02}O_{1+\delta}$. Stratification which is observed sometimes for continuous series of solid solutions $A^{II}B^{VI}$ (sphalerite structural type), was for the first time reported [102] for the wurtzite-type limited solid solutions $Zn_{1-x}Co_xO_{1+\delta}$.

Only antiferromagnetic ordering occurs in the solid solutions $Zn_{1-x}Co_xO_{1+\delta}$ ($x \leqslant 0.2$); it retains even upon introducing ferromagnetic oxides; stratification disappears on long-term annealing; manifestation of ferromagnetism in the polycrystals and ceramics based on $Zn_{1-x}Co_xO_{1+\delta}$ is most probably due to violation of homogeneity or to the presence of impurities.[106] However, these conclusions concern only large $Zn_{1-x}Co_xO_{1+\delta}$ crystallites. In the metastable state, the homogeneity region of the wurtzite-type solid solution can extend considerably,[107] whereas in the case of films, taking into account random population of crystallographic positions, the notion 'single-phase system' becomes senseless as the film thickness decreases.

Thus, the preparation of a homogeneous 'hybrid' FS retaining ferromagnetic ordering at 400 – 450 K and a partial pressure of oxygen of 20 kPa is still a topical task.[108] Studies in this field are of particular interest because the size of electronic devices should reduce considerably when using FS nanofilms as working units of nanocircuits.

IV. Search for DMS phases in the systems Mg – Ga(Al) – Fe – O

Studies of the Zn – Co – O system revealed that an atypical property, *viz.*, ferromagnetic ordering, cannot be imparted to the structure. Not rejecting the DMS approach, we tried to search for continuous solid solutions using the concept of isostructural unit cells of the semiconductor oxide matrix and the ferromagnetic oxide being dissolved in the matrix. The spinel $MgAl_2O_4$ was chosen to be a basic structure typical of not only semiconductors and dielectrics, but also ferrites.[109]

A binary ferrite Fe_3O_4 (magnetite) retains ferromagnetic ordering up to 850 K. It has a high conductivity ($> 10^4$ S m^{-1}) which is due to electron exchange between Fe^{2+} and Fe^{3+} (see Ref. 110) and varies insignificantly in the temperature range 150 – 1700 K.[111] However, the use of Fe_3O_4 for the preparation of homogeneous DMS materials faces some problems, which concern first of all control of the partial pressure of oxygen during the synthesis and cooling to keep the Fe^{2+}/Fe^{3+} ion ratio in magnetite constant. The isoconcentrates $p_{O_2} = f(T)_{x=\text{const}}$ of the DMS materials based on $Fe_3O_{4+\delta}$ are unknown and moreover, cooling of such solid solutions following the isoconcentrates is difficult, taking into account the nonstoichiometry with respect to oxygen ($4+\delta$). An attempt

to obtain $Zn_xFe_{3-x}O_4$ films ($0 \leqslant x \leqslant 0.9$) on MgO(001) substrates by molecular beam epitaxy in argon atmosphere or in $Ar + O_2$ mixture was reported.[112] It is noteworthy that the initial ceramics $Zn_xFe_{3-x}O_4$ was not analyzed and possible interaction of zinc spinel with MgO was not considered.

Experiments on the preparation of DMS phases in the system $ZnGa_2O_4 - Fe_3O_4$ gave a $(ZnGa_2O_4)_{0.85}(Fe_3O_4)_{0.15}$ solid solution with $T_C \approx 200$ K and a bandgap of 4.1 eV.[113]

The cation distribution in solid solutions $(Fe_3O_4)_x.(MgAl_2O_4)_{1-x}$ was studied [114–119] using quenching of samples annealed at $T = 1573-1673$ K and $p_{O_2} = 2-10$ Pa. These parameters in the $P-T$ diagram of the system $Fe-O$ [64] correspond to the existence region of magnetite; a decrease in temperature and an increase in pressure lead to the oxidation Fe_3O_4 to Fe_2O_3 and to formation of a solid solution of $(\gamma\text{-}Fe_{8/3}O_4)_x(MgAl_2O_4)_{1-x}$ with the defect γ-Fe_2O_3 (maghemite) having the spinel structure.[114] The conductivities of $(Fe_3O_4)_x(MgAl_2O_4)_{1-x}$ on heating and on cooling measured in the temperature range 873–1673 K ($p_{O_2} = 2$ Pa) coincide within experimental error,[115] but the temperature dependences of the magnetic susceptibility $\chi(T)$ measured in air ($p_{O_2} \approx 2 \times 10^4$ Pa) in the temperature range 673–923 K appeared to be irreversible because of cation ordering and stratification.[118] The T_C values determined from the $\chi(T)$ dependences for the samples annealed at temperatures below 923 K were more than 70 K higher than the T_C values of the samples quenched from 1673 K at the same cation composition; a mixture of ferromagnetic and paramagnetic phases was isolated in the concentration range $0.55 < x < 0.7$.[118] Formally, stratification of solid solutions upon annealing can be explained by a kind of competition, namely, Fe_3O_4 'tends' to organize randomly distributed cations to form a 'reverse' spinel $(Fe^{3+}).[Fe^{2+}Fe^{3+}]O_4$,[110] whereas $MgAl_2O_4$ 'tends' to form a 'normal' spinel $(Mg^{2+})[Al^{3+}]_2O_4$ (parentheses and square brackets denote that cations are in the tetrahedral and octahedral environment of oxygen anions, respectively).[119]

Using $MgFe_2O_4$ instead of Fe_3O_4, one can fix the oxidation state of Fe^{3+} cations; also, stable $MgFe_2O_4$ can be prepared and annealed in air.[110] The synthesis conditions of a single-phase material with the stoichiometric ratio $Mg:Fe = 1:2$ are determined by not only the choice of precursors,[110] but also their dispersion.[120] Attempts to replace Fe^{3+} by Al^{3+} in $MgFe_2O_4$ to obtain ferrites for UHF devices by 'magnetic dilution' showed that solid solutions $Mg(Fe_{1-x}Al_x)_2O_4$ synthesized from oxides contain impurity phases.[121] Nevertheless, it is oxides that were used to obtain solid solutions with $x = 0.0-0.7$ after 12 h annealing at 1225 K.[122] The concentration dependences $a(x)$, where a is the lattice constant, exactly obeyed the Vegard rule and the $T_C(x)$ dependences for the solid solutions with $x \geqslant 0.15$ were almost linear; nevertheless, an increase in temperature from 300 to 500 K led to abnormal conductivity drop by 3–4 orders of magnitude.[122]

To avoid stratification when preparing a homogeneous DMS material, two 'reverse' spinels were used, namely, magnetic $MgFe_2O_4$ and dielectric $MgGa_2O_4$.[123, 124]

Self-propagating high-temperature synthesis [125] was used to obtain single-phase materials $Mg(Fe_{1-x}Ga_x)_2.O_{4+\delta}$.[126] To a solution of magnesium, gallium and iron in nitric acid, citric acid was added and the solution was concentrated at 400–500 K until the formation of a dense mass. Further heating was accompanied by a self-propagating combustion reaction with the formation of a brown finely dispersed powder which was then annealed at 1223–1273 K for 20 h and cooled with a furnace for ~4–5 h.

The bandgap of $Mg(Fe_{1-x}Ga_x)_2O_{4+\delta}$ was determined from the diffuse scattering spectra, namely, monochromatic radiation reflected from thin polycrystalline layer of the sample on a sapphire holder was analyzed. The contribution of weak luminescence of samples to the diffuse scattering was ignored. The absorbance of the material (α) in relative units was calculated from the relation

$$\alpha = \ln \frac{I_{sapp}}{I_{samp}},$$

where I_{sapp} and I_{samp} are the diffuse reflection intensities of the matted sapphire and the sample under study, respectively.

The concentration dependences of the lattice constant of solid solutions $Mg(Fe_{1-x}Ga_x)_2O_{4+\delta}$ are presented in Fig. 7. The patterns of the $a(1-x)$ curves are mainly governed by the method of synthesis of the solid solutions rather than the heat treatment parameters (annealing temperature and duration, cooling rate).

A feature of solid-phase synthesis of samples from oxides or from mixtures of magnesium ferrite with gallate in air (1373 K) followed by quenching or cooling at a rate of 10 K h^{-1} the curves $a(1-x)$ is the kink in the curves $a(1-x)$ at $1-x = 0.5-0.6$,[127] which indicates that the system is near the stratification region. Annealing in air (12 h, 1673 K) of compacted oxides prepared from a dried and calcined mixture of hydroxides led to two solid solutions based on $MgGa_2O_4$ and on $MgFe_2O_4$;[128] this confirms the possibility for stratification to occur at high temperatures. An almost ideal dependence $a(1-x)$ was obtained for the samples synthesized from oxides at 1273 K after 350-h (!) annealing and subsequent quenching in liquid nitrogen.[129] However, the operating temperature range and service life of such a metastable ceramic material are unknown while the use of the material in the form of a film seems to be problematic.

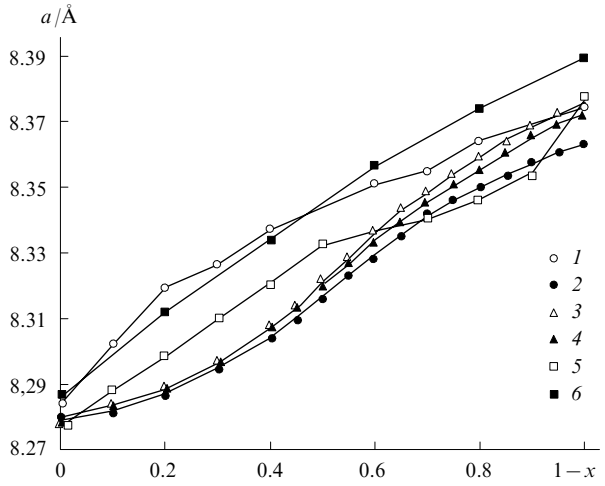


Figure 7. Concentration dependences of the lattice constant in $Mg(Fe_{1-x}Ga_x)_2O_{4+\delta}$.
Data taken from Ref. 123 (*1*), quenching from 1373 K (*2*), cooling from 1373 K (*3*), cooling from 1173 K (*4*),[127] annealing at 1673 K (*5*) [128] and annealing at 1273 K (350 h) followed by quenching in liquid nitrogen (*6*).[129]

The use of citric acid as reducing agent in the synthesis of $Mg(Fe_{1-x}Ga_x)_2O_{4+\delta}$ led to positive deviations from the Vegard rule for all compositions.[126] This is probably due to the cation reduction from Fe^{3+} to Fe^{2+}. Samples heated to 573 K still remained single-phase compositions; this indicated their thermal stability, but did not reject the possibility of being in the metastable state.

The magnetic field dependences of the specific magnetic moments (m) of the $MgFe_2O_{4+\delta}$ and $Mg(Fe_{0.8}Ga_{0.2})_2O_{4+\delta}$ samples reach saturation at low external fields (from 0.3 to 0.5 T, see Fig. 8). The saturation magnetization of the substituted sample $Mg(Fe_{0.8}Ga_{0.2})_2O_{4+\delta}$ (~ 30 A m^2 kg^{-1}) is considerably higher than that of pure ferrite $MgFe_2O_{4+\delta}$

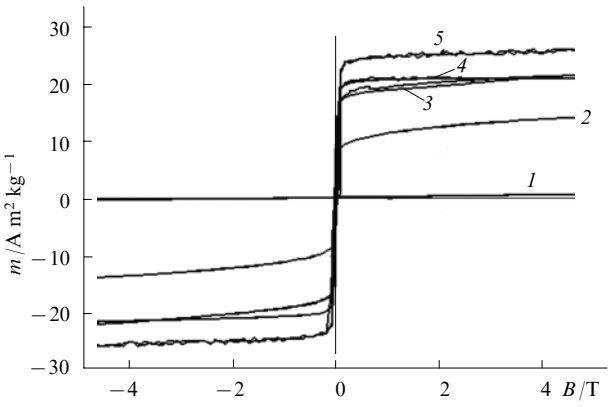


Figure 8. Magnetic field dependences of the magnetic moments of $Mg(Fe_{0.2}Ga_{0.8})_2O_{4+\delta}$ (*1*), $Mg(Fe_{0.65}Ga_{0.35})_2O_{4+\delta}$ (*2*), $Mg(Fe_{0.7}Ga_{0.3})_2O_{4+\delta}$ (*3*), $MgFe_2O_{4+\delta}$ (*4*) and $Mg(Fe_{0.8}Ga_{0.2})_2O_{4+\delta}$ (*5*).[105]

(~ 20 A m^2 kg^{-1}). Probably, Ga^{3+} cations ($x < 0.3$) displace the Fe^{3+} and Mg^{2+} cations from tetrahedral to octahedral sites, and the spinel becomes less 'reverse' with respect to Fe^{3+} (Refs 127 and 128). The magnetizations of $Mg(Fe_{0.7}Ga_{0.3})_2O_{4+\delta}$ and $Mg(Fe_{0.65}Ga_{0.35})_2O_{4+\delta}$ do not reach the saturation magnetization values even in an external magnetic field of 5 T. This suggests magnetic inhomogeneity of the samples analyzed, *e.g.*, the presence of a mixture of ferromagnetic and paramagnetic fractions. A similar phenomenon is observed in the annealing of $(Fe_3O_4)_x(MgAl_2O_4)_{1-x}$ samples ($x = 0.55-0.7$), namely, the same spinel structure[115] comprises a mixture of ferromagnetic and paramagnetic phases.[119]

The sample $Mg(Fe_{0.2}Ga_{0.8})_2O_{4+\delta}$ shows a weak response to external magnetic field. This can be explained by the attainment of concentration identity with respect to Fe^{3+} in the tetrahedral and octahedral sites upon cationic substitution and, as a consequence, by compensation of the magnetic moments.

All polycrystalline samples are magnetically soft materials. The coercive force (F) of the spinels under study is low:

Sample	F/T
$MgFe_2O_{4+\delta}$	~ 0.0085
$Mg(Fe_{0.8}Ga_{0.2})_2O_{4+\delta}$	~ 0.0188
$Mg(Fe_{0.7}Ga_{0.3})_2O_{4+\delta}$	~ 0.0095
$Mg(Fe_{0.65}Ga_{0.35})_2O_{4+\delta}$	~ 0.0086
$Mg(Fe_{0.2}Ga_{0.8})_2O_{4+\delta}$	~ 0.0191

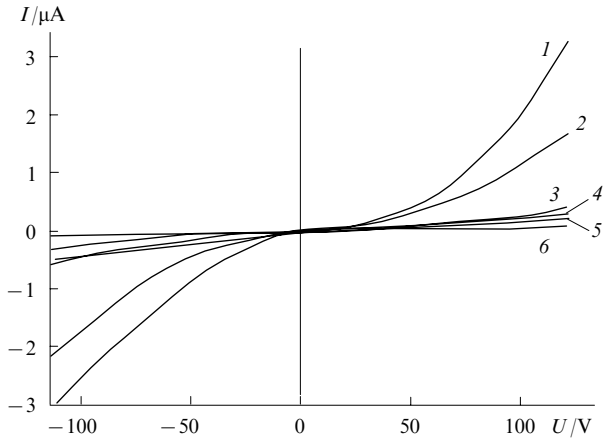


Figure 9. Voltammograms of $Mg(Fe_{0.8}Ga_{0.2})_2O_{4+\delta}$ (*1*), $Mg(Fe_{0.7}Ga_{0.3})_2O_{4+\delta}$ (*2*), $Mg(Fe_{0.65}Ga_{0.35})_2O_{4+\delta}$ (*3*), $Mg(Fe_{0.2}Ga_{0.8})_2O_{4+\delta}$ (*4*), $MgFe_2O_{4+\delta}$ (*5*) and $MgGa_2O_4$ (*6*) samples.[105]

The $I-V$ curves of $Mg(Fe_{1-x}Ga_x)_2O_{4+\delta}$ were obtained at room temperature. The direct and reverse branches of the voltammograms shown in Fig. 9 are symmetrical for all samples. This is an indication of a homogeneous medium.

The conductivities of compacted powders $Mg(Fe_{0.7}Ga_{0.3})_2O_{4+\delta}$ and $Mg(Fe_{0.8}Ga_{0.2})_2O_{4+\delta}$ are an order of magnitude higher than those of other solid solutions. This is probably due to an increase in the surface concentration of Fe^{2+} ions. As the voltage increased from 50 to 100 V, the conductivity of magnesium ferrite increased from 3×10^{-9} to 7×10^{-9} S m^{-1} [*cf.* the ranges from 2.5×10^{-8} to 4×10^{-8} S m^{-1} for $Mg(Fe_{0.7}Ga_{0.3})_2O_{4+\delta}$ and from 4×10^{-8} to 8×10^{-8} S m^{-1} for $Mg(Fe_{0.8}Ga_{0.2})_2$. $.O_{4+\delta}$]. At voltages above 100 V, the conductivity of $Mg(Fe_{0.8}Ga_{0.2})_2O_{4+\delta}$ almost doubled. Probably, the current flowing across grain boundaries increases at so high voltages. This is confirmed by the accumulation of static charge. In some cases, removal of static charge was accompanied by sparking and characteristic traces of streamers along the surfaces of grains.

Magnesium ferrite exhibits the properties of a semiconductor and, to some extent, a semi-insulator, whereas pure magnesium gallate is a dielectric. The α^2 values determined from the diffuse scattering intensity ratios of sapphire and of the samples under study are shown in Fig. 10. The energy values correspond to regions of absorption of electromagnetic radiation with a particular wavelength. These data were used to evaluate the bandgap (E_g) of the $Mg(Fe_{1-x}Ga_x)_2O_{4+\delta}$ samples. All compositions, except the initial one, are characterized by two E_g values: 1.9 and 2.1 eV for $MgFe_2O_{4+\delta}$; 1.9 and 2.4 eV for $Mg(Fe_{0.8}Ga_{0.2})_2O_{4+\delta}$, $Mg(Fe_{0.7}Ga_{0.3})_2O_{4+\delta}$ and $Mg(Fe_{0.65}Ga_{0.35})_2O_{4+\delta}$; and 2.3 and 2.9 eV for $Mg(Fe_{0.2}Ga_{0.8})_2O_{4+\delta}$. The initial $MgGa_2O_4$ was characterized by $E_g = 3.0$ eV. This experimental fact cannot be interpreted unambiguously until actual distribution of Mg^{2+}, Ga^{3+}, Fe^{3+} and Fe^{2+} cations over tetrahedral and octahedral sites in the spinels of different compositions is known.[127, 128]

Studies on the magnetic and electrophysical properties of $Mg(Fe_{0.8}Ga_{0.2})_2O_{4+\delta}$ showed that this composition is optimum for obtaining diluted magnetic semiconductors in

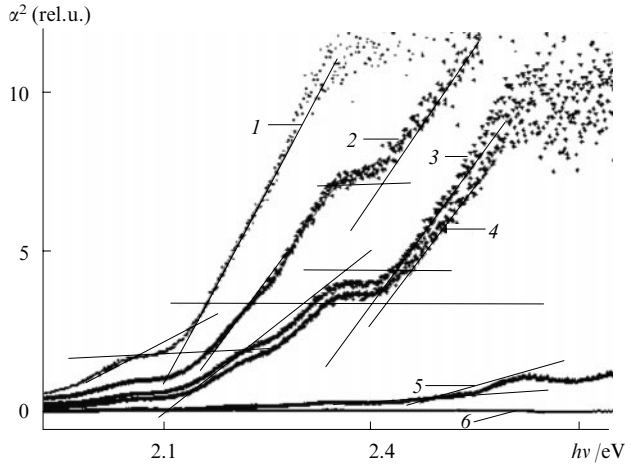


Figure 10. Absorption spectra of $MgFe_2O_{4+\delta}$ (*1*), $Mg(Fe_{0.8}Ga_{0.2})_2O_{4+\delta}$ (*2*), $Mg(Fe_{0.65}Ga_{0.35})_2O_{4+\delta}$ (*3*), $Mg(Fe_{0.7}Ga_{0.3})_2O_{4+\delta}$ (*4*), $Mg(Fe_{0.2}Ga_{0.8})_2O_{4+\delta}$ (*5*) and $MgGa_2O_4$ (*6*).[105]

the form of ceramics, single crystals or films for application in spintronics devices.[103]

The composition line $MgFe_2O_4-MgGa_2O_4$ only bounds the tetragon $Fe_3O_4-MgFe_2O_4-MgGa_2O_4-FeGa_2O_4$ within the concentration tetrahedron Mg–Ga–Fe–O (Fig. 11); all complex oxides belonging to this tetragon can crystallize in the spinel structural type. It cannot be ruled out that the physicochemical properties of these spinels to a greater extent meet the requirements imposed on the materials for spintronics compared to the properties of $Mg(Fe_{0.8}Ga_{0.2})_2O_{4+\delta}$.

To set up a comprehensive study,[130] the conditions for preparation of homogeneous spinels in the concentration tetragon $Fe_3O_4-MgFe_2O_4-MgGa_2O_4-FeGa_2O_4$ were assessed first of all.

Unlike analytical description of the phase states, the topological description does not require a physical model,

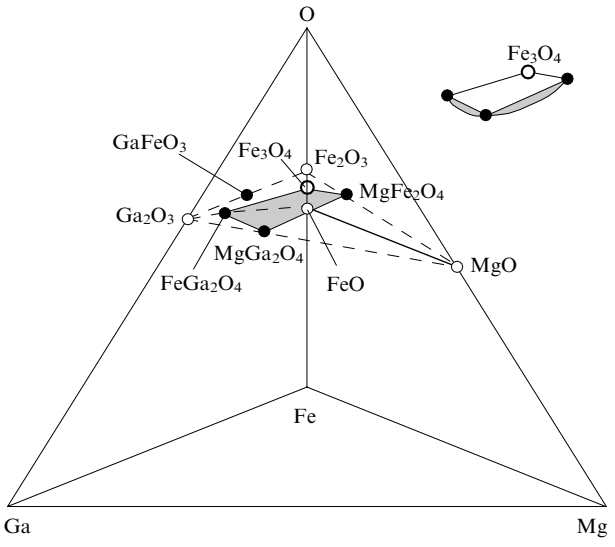


Figure 11. Spinel region in the concentration tetrahedron Mg–Ga–Fe–O.[103]

which makes the technique versatile in the studies of multicomponent systems.[130] Despite the fact that the region of compositions of complex oxides (ignoring nonstoichiometry with respect to oxygen) forming spinels, namely, the tetragon $Fe_3O_4-MgFe_2O_4-MgGa_2O_4-FeGa_2O_4$ (see Fig. 11), does not span the entire region of solid solutions, we will restrict ourselves to this approximation and use it in a particular concentration tetrahedron $MgO-Ga_2O_3-FeO-Fe_2O_3$ (Fig. 12).

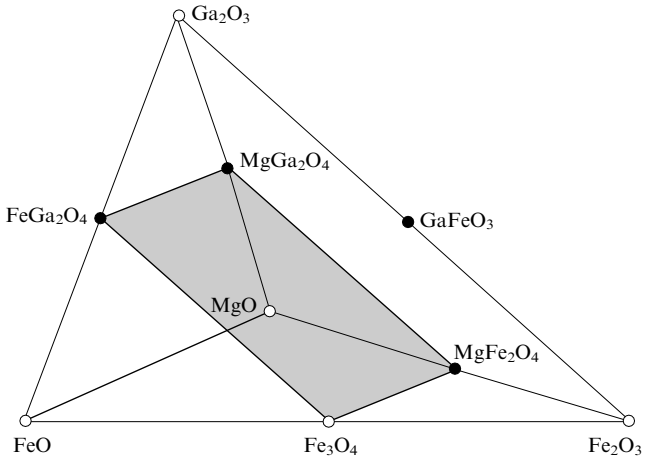


Figure 12. Spinel region in the tetrahedron $MgO-Ga_2O_3-FeO-Fe_2O_3$ ($T < 1300$ K).[130]

Spinels can be obtained at any ratio Mg : Ga : Fe in the compositions confined within the tetragon $Fe_3O_4-MgFe_2O_4-MgGa_2O_4-FeGa_2O_4$ (see Figs 11 and 12). There are two decisive and limiting factors, *viz*., the temperature and the partial pressure of oxygen over solid solutions. However, it is hardly expedient to study systematically the dependences $p_{O_2}-T$ for the two-phase spinel–oxygen states in the system Mg–Ga–Fe–O. To assess, it is sufficient to use the $P-T-x$ phase diagram of the system Fe–O,[131] which defines the existence regions of wüstite $FeO_{1+\delta}$, magnetite $Fe_3O_{4+\delta}$ and hematite $Fe_2O_{3+\delta}$.

One can believe that Fig. 12 describes the concentration space of spinel to 1300 K. In the temperature range 1300–1700 K (prior to melting), the phase volume of spinel is transformed to a hexagon *1–2*–$MgFe_2O_4$–*3–4–5–6* (Fig. 13). Magnetite Fe_3O_4 is characterized by noticeable oxygen solubility which can be interpreted as the limited solubility (to 10 mol.%) of metastable maghemite γ-Fe_2O_3 (more exactly, γ-$Fe_{8/3}O_4$ with the defect spinel structure).[132] The nonstoichiometry of the magnetite spinel with respect to oxygen (see Fig. 13) decreases upon replacement of Fe^{2+} by Mg^{2+} cations and in the boundary system $MgO-Fe_2O_3$ one gets a constant chemical composition $Mg_{1.092}Fe_2O_4$ which is almost independent of the partial pressure of oxygen.[110, 133, 134] Interestingly, the stoichiometric composition $MgFe_2O_4$ is a mixture of spinel and hematite (α-Fe_2O_3).

In addition to magnesium ferrite, magnetite forms a solid solution with iron gallate $FeGa_2O_4$ (Ref. 135) which can dissolve the superstoichiometric oxide Ga_2O_3 (according to estimates, up to 5 mol.%). It cannot be ruled out that spinel $Fe(Fe_{1-x}Ga_x)_2O_{4+\delta}$ has a stratification region as indicated by the concentration dependences of the lattice

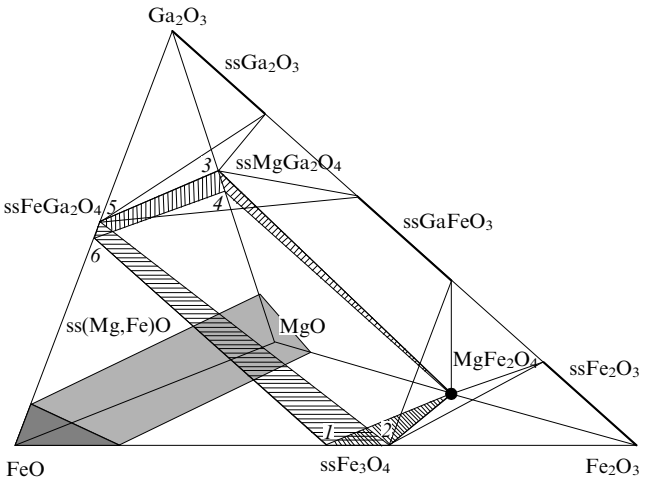


Figure 13. Model for the phase volumes of solid solutions in the concentration tetrahedron $MgO-Ga_2O_3-FeO-Fe_2O_3$. Hexahedron *1–2–*$MgFe_2O_4$*–3–4–5–6* represents the phase volume of spinel.[130]

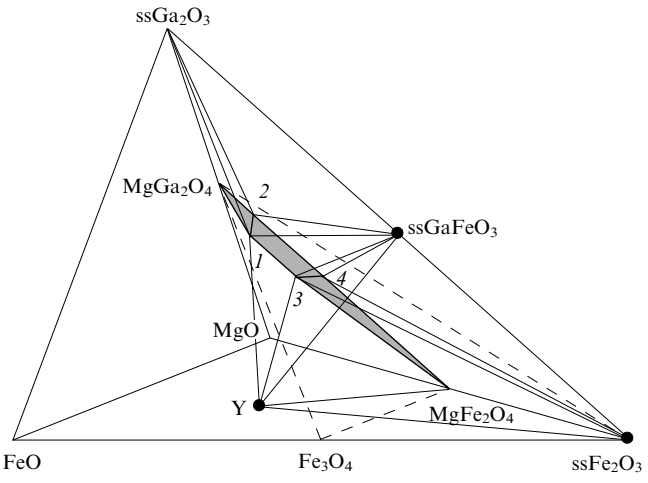


Figure 14. Isobaric isothermal concentration phase diagram of the system $MgO-Ga_2O_3-FeO-Fe_2O_3$.[130] For notations *1–4*, see text.

constant and Curie temperature.[136] Correspondingly, the phase based on $MgGa_2O_4$, the last compound from the 'spinel tetragon' compositions, dissolves 1 mol.%–2 mol.% MgO and to 10 mol.% Ga_2O_3 in the temperature range 1300–1700 K.[137]

In addition to the spinel-type solid solution, a limited solid solution based on the orthoferrite $GaFeO_3$, mutual solid solutions of α-Fe_2O_3 and β-Ga_2O_3,[135] and a continuous solid solution of magnesium wüstite are formed in the system $Mg-Ga-Fe-O$.[138] The solubilities of MgO and FeO in α-Fe_2O_3,[134] as well that of MgO in β-Ga_2O_3 is negligible.[137] It is admissible to assume, by analogy with the systems $NiO-Ga_2O_3$ (Ref. 137) and $FeO-Al_2O_3$,[139] that the solubility of FeO in β-Ga_2O_3 is also low.

Contrary to this, the solubility of Ga_2O_3 and Fe_2O_3 in periclase MgO or in wüstite FeO can be as high as 15 mol.%.[137, 139–141] Thus, magnesium wüstite, unlike the limited solid solutions based on α-Fe_2O_3, orthoferrite $GaFeO_3$ and β-Ga_2O_3, occupies a rather large volume in the quaternary system $MgO-Ga_2O_3-FeO-Fe_2O_3$.

Figure 13 presents the model for the phase volumes of solid solutions in the concentration tetrahedron $MgO-Ga_2O_3-FeO-Fe_2O_3$. The isobaric isothermal sections for these phase volumes will vary depending on the pressure and temperature.

To determine the concentration space occupied by the spinel phase at p_{O_2} = 21 kPa and T = 1273 K in the tetrahedron $MgO-Ga_2O_3-FeO-Fe_2O_3$, the compositions conditionally belonging to the diagonals $MgGa_2O_4-Fe_3O_4$ and $MgFe_2O_4-FeGa_2O_4$ were studied (see Fig. 12).[130]

Polycrystalline samples with the nominal compositions $Mg_{1-x}Ga_{2-2x}Fe_{3x}O_4$ and $Mg_{1-x}Ga_{2x}Fe_{2-x}O_4$ with an increment x = 0.1 were prepared by self-propagating high-temperature synthesis.[125]

Based on the results obtained, a fragment of the isobaric isothermal phase diagram of the system $MgO-Ga_2O_3-FeO-Fe_2O_3$ at p_{O_2} = 21 kPa and T = 1273 K was plotted (Fig. 14). The spinel homogeneity region is bounded by the $MgGa_2O_4$*–1–3–*$MgFe_2O_4$*–4–2* contour (given in grey); the $MgGa_2O_4$*–1–2*, *1–2–3–4* and *3–4–*$MgFe_2O_4$ segments correspond to the spinel compositions in two-phase equilibria with the solid solutions based on Ga_2O_3, $GaFeO_3$ and Fe_2O_3, respectively; the lines *1–2*, *3–4*, *1–3* and *3–*$MgFeO_4$ correspond to variation of the spinel composition in three-phase equilibria spinel–$ssGa_2O_3$–$ssGaFeO_3$, spinel–$ssGaFeO_3$–$ssFe_2O_3$, spinel–$ssGaFeO_3$–phase Y (isostructural to $Ca_2Fe_7O_{11}$, see Ref. 142) and spinel–$ssFe_2O_3$–phase Y. Point *3* corresponds to the spinel composition (a = 8.29–8.33 Å) in the four-phase equilibrium spinel–$GaFeO_3$–Fe_2O_3–Y.

None of the samples studied showed stratification of spinels similar to that observed in the system $Mg-Al-Fe-O$ under isobaric isothermal conditions.[143, 144] Based on experimental data, stratification is retained at low partial pressures of oxygen for spinels from the tetragon $Fe_3O_4-MgAl_2O_4-MgFe_2O_4-FeAl_2O_4$.[115] The main reason for stratification is that the spinels based on $MgAl_2O_4$ and $FeAl_2O_4$ are 'normal' spinels while those based on Fe_3O_4 and $MgFe_2O_4$ are the 'reverse' ones.[145]

Stratification of the 'reverse' spinels formed in the system $Mg-Ge-Fe-O$ is not observed at least in the stable state. Taking into account the fact that the homogeneity of spinels is retained in a wide range of compositions, preparation of homogeneous ceramics and films for microelectronics devices becomes possible.

Only measurements using a single crystal or a homogeneous film can provide a direct proof of formation of a homogeneous DMS material based on the limited solid solution. In the case of continuous solid solutions, some conclusions about the formation of homogeneous DMS materials can be drawn based on indirect data, *e.g.*, monotonic variation of the lattice constants and Curie temperature depending on the chemical composition.

A modified DMS approach, *i.e.*, dissolution of a semiconductor (insulator) in the ferromagnetic matrix until attainment of optimum electrophysical properties, was used in the experiments with continuous solid solutions formed by isomorphous semiconductor spinels and ferrites. The advantage of the modified approach is due to the fact that interphase boundaries strongly influence the 'behaviour' of charge carriers, which allows one to level the effect of possible random impurities on the semiconductor properties. To avoid stratification of solid solutions, the pair

'semiconductor – ferromagnetic material' was chosen taking into account the extent to which both spinels can be treated as 'reverse' ones.

V. Homogeneous complex metal – oxide films

Barium hexaferrite ($BaFe_{12}O_{19}$) films on heat-treated single-crystalline silicon substrates were obtained by successive ion beam sputtering of $BaFe_2O_4$ and α-Fe_2O_3 targets in argon or oxygen.[146] It was established that single-phase $BaFe_{12}O_{19}$ films crystallize on annealing only when preliminarily coated with an α-Fe_2O_3 buffer layer deposited during a continuous vacuum cycle. The protective α-Fe_2O_3 layer precludes the formation of barium silicates and solid-phase reactions proceed within $BaFe_2O_4/\alpha$-$Fe_2O_3/SiO_2/Si$ interfaces.

The combined use of ion-plasma methods (treatment of substrates in microwave plasma; growth of metal – oxide layers of specified complex compositions by ion beam sputtering in oxygen or argon atmosphere)[147–149] made it possible to obtain spinel films on silicon using $Mg(Fe_{0.8}Ga_{0.2})_2O_{4+\delta}$ ceramic targets.[150]

Polycrystalline samples of nominal chemical composition $Mg(Fe_{0.8}Ga_{0.2})_2O_{4+\delta}$ were obtained by self-propagating high-temperature synthesis,[125] pressed and annealed in air at 1023 K.

Eight polyhedral ceramic samples of size $5 \times 5 \times 80$ mm were used as targets in the preparation of films in the system Mg – Ga – Fe – O by ion beam sputtering. According to the X-ray diffraction pattern shown in Fig. 15, the ceramic samples had the spinel structure with the lattice constant $a = 0.837$ nm and showed the characteristic reflections (220) and (311) at 30.24 and 35.6°, respectively. Impurity phases were present in trace amounts.

From the magnetic field dependences (Fig. 16) it follows that the specific magnetic moment of $Mg(Fe_{0.8}Ga_{0.2})_2O_{4+\delta}$ ceramics reaches a saturation value at a low external field (0.3 – 0.5 T). The saturation magnetization at 4 K is about 50 A m^2 kg^{-1}; at 300 K, it decreases to 30 A m^2 kg^{-1} because of temperature-induced disordering of the magnetic structure.

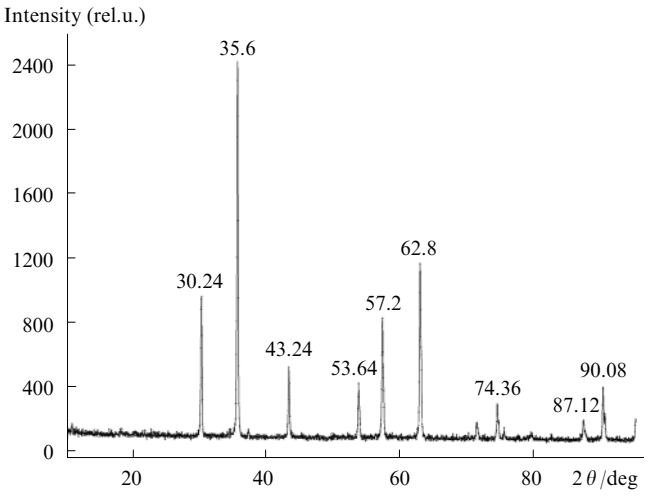


Figure 15. X-Ray diffraction pattern of $Mg(Fe_{0.8}Ga_{0.2})_2O_{4+\delta}$ ceramics.[150]

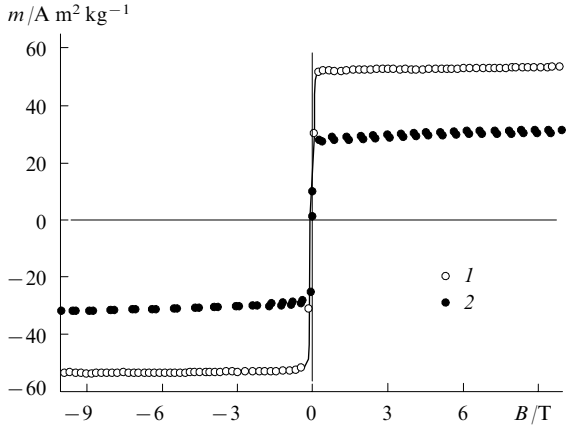


Figure 16. Magnetic field dependences of the specific magnetic moment of $Mg(Fe_{0.8}Ga_{0.2})_2O_{4+\delta}$ ceramics measured at 4 (*1*) and 300 K (*2*).[150]

The temperature dependences of the specific magnetic moment on cooling with no external magnetic field applied and in a weak magnetic field (Fig. 17) almost match each other, being nearly linear and thus indicating a magnetically homogeneous structure of the sample. From the temperature dependences of the specific magnetic moment (Fig. 18 *a*) and its squared value (Fig. 18 *b*) in the range 300 – 650 K, the Curie temperature of $Mg(Fe_{0.8}Ga_{0.2})_2O_{4+\delta}$ ceramics is ~490 K. The calculated effective magnetic moment per Fe^{3+} ion is 5 μ_B (for the electronic configuration $3d^5$); however, based on the experimental data for the $Mg(Fe_{0.8}Ga_{0.2})_2O_{4+\delta}$ sample, it is only 1.4 μ_B (28% of the calculated value). Discrepancies may be due to the following reasons:

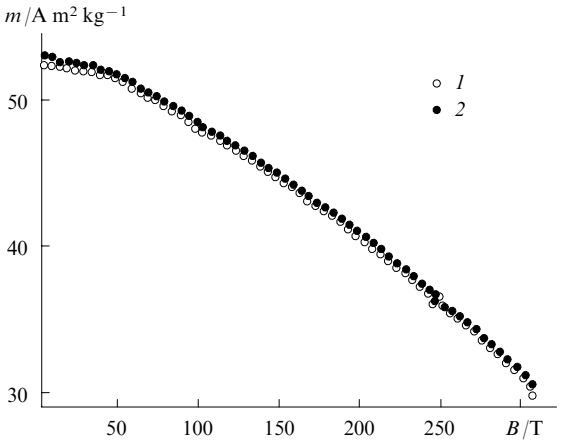


Figure 17. Temperature dependences of the specific magnetic moment of $Mg(Fe_{0.8}Ga_{0.2})_2O_4$ ceramics.[150]
Cooling regime: zero-field cooling (*1*) and cooling in a weak (at most 0.1 T) magnetic field (*2*).

— co-existence of two magnetic phases within the spinel structure;

— non-collinearity of the magnetic moment vectors in the case of a single magnetic phase (so-called sperimagnetism);

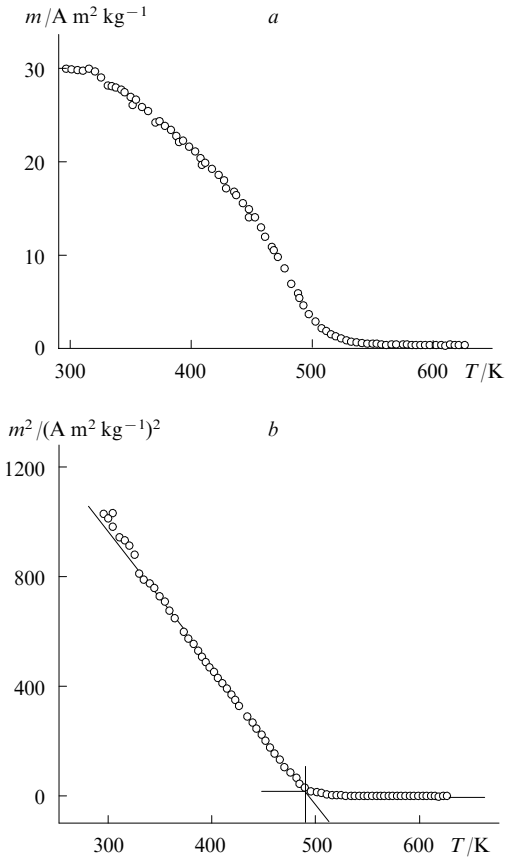


Figure 18. Temperature dependences of the specific magnetic moment (*a*) and its squared value (*b*) for $Mg(Fe_{0.8}Ga_{0.2})_2O_{4+\delta}$ ceramics.[150]

— compensation of the magnetic moments of the spinel A- and B-sublattices due to replacement of iron ions by gallium ions in octahedral sites.

The data presented in Figs 17 and 18 (magnetic homogeneity of the sample) and the underestimated value of the effective magnetic moment per iron ion support the third case.

Targets were sputtered with argon or oxygen ions for a period of 1.5 h onto single-crystalline silicon wafers 76 mm in diameter heated to 400 K under the operating pressure (at most 0.2 Pa) and a limiting rarefaction of 0.01 Pa.[150] Prior to film deposition, the silicon wafers were treated with microwave oxygen plasma[148] to remove organic components and substances adsorbed on the silicon surface. The film growth rate was about 135 nm h^{-1}.

Silicon wafers with $Mg(Fe_{0.8}Ga_{0.2})_2O_{4+\delta}$ deposits whose thickness gradually increased from 40 to 280 nm were cut into rectangular samples 5×10 mm in size; the film thickness varied within 20%. The samples thus obtained were annealed for 30 min in air at 973, 1073, 1173 and 1273 K.

Films prepared as a result of sputtering of a $Mg(Fe_{0.8}Ga_{0.2})_2O_{4+\delta}$ ceramic target with argon or oxygen ions were annealed at 1273 and 1173 K. A comparison of the X-ray diffraction patterns (Figs 19 and 20) showed that the most promising films for spintronics applications are those produced by sputtering with oxygen ions until a deposit thickness over 0.2 μm is reached and then annealed at 1173 K. The films grown on silicon by argon-ion sputtering of the target with subsequent annealing at 1273 K have a non-spinel structure [most probably, this was a solid solution based on gallium orthoferrite $GaFeO_3$ (see Fig. 19)]. Sputtering of the target with oxygen ions did not lead to the formation of spinel in as-deposited layers (see Fig. 20 *a*). Annealing of the samples at 1273 K produced an impurity phase (most probably, hematite α-Fe_2O_3) (see Fig. 20 *c*). Having lowered the annealing temperature to 1173 K, a spinel film over 0.2 μm thick was obtained by

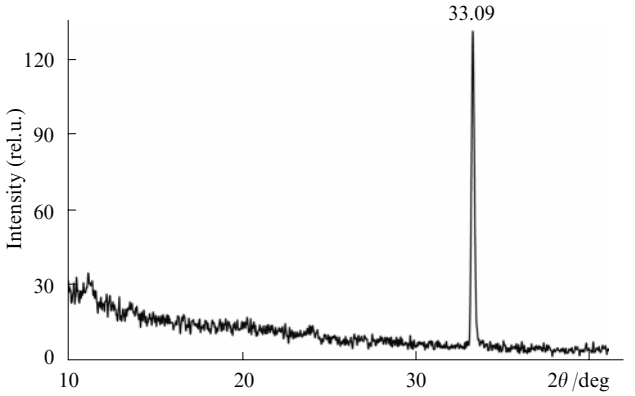


Figure 19. X-Ray diffraction pattern of a film sample obtained by sputtering of $Mg(Fe_{0.8}Ga_{0.2})_2O_{4+\delta}$ target with argon ions and annealed in air at 1273 K.[150]

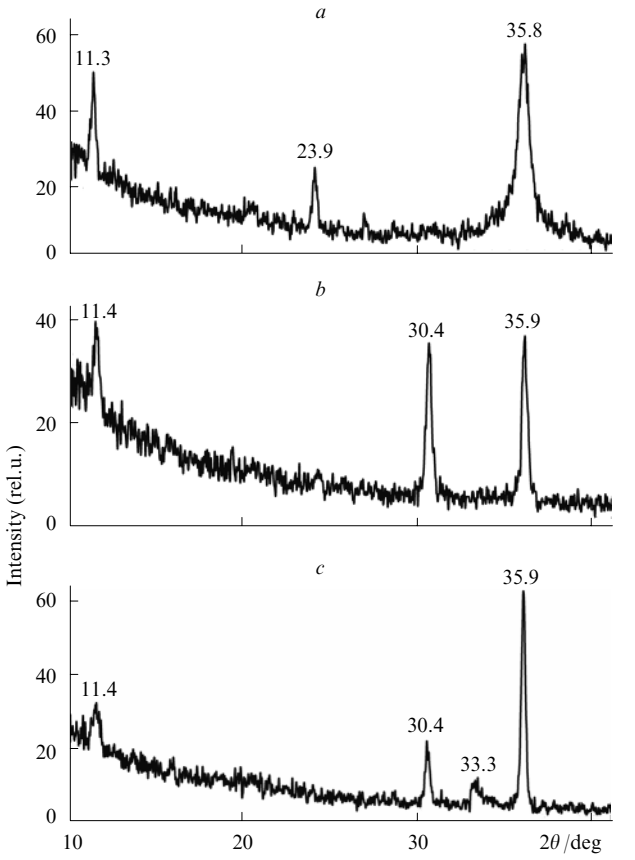


Figure 20. X-Ray diffraction patterns of film samples prepared by sputtering of $Mg(Fe_{0.8}Ga_{0.2})_2O_{4+\delta}$ target with oxygen ions.[150] Initial sample (*a*), after annealing at 1173 K (*b*) and after annealing at 1273 K (*c*).

sputtering of the target with oxygen ions (see Fig. 20 *b*); the film structure was similar to that of $Mg(Fe_{0.8}Ga_{0.2})_2O_4$ ceramics (see Fig. 15).

Using a vibrating magnetometer, the magnetic field dependences of the specific magnetic moment at 5 K in external fields to ±3 T were obtained for the samples prepared by sputtering of $Mg(Fe_{0.8}Ga_{0.2})_2O_{4+\delta}$ target with oxygen ions and subsequently annealed at 973 and 1173 K in air (Fig. 21). The highest specific magnetic moments of the film samples were ~1.26 (973 K) and ~4.7 A m^2 kg^{-1} (1173 K); coercive force was ~0.16 T (973 K) in the former and ~0.095 T (1173 K) in the latter case.

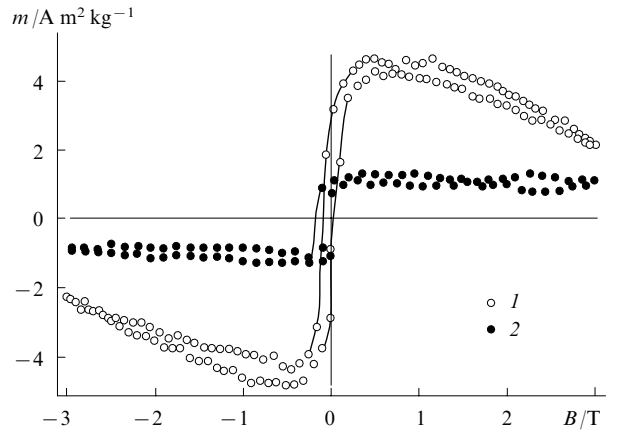


Figure 21. Magnetic field dependences of the specific magnetic moment of film samples prepared by sputtering of $Mg(Fe_{0.8}Ga_{0.2})_2O_{4+\delta}$ target with oxygen ions and annealed at 1173 (*1*) and 973 K (*2*).[150]

Sputtering of a $Mg(Fe_{0.8}Ga_{0.2})_2O_{4+\delta}$ target with a beam of 1.2-kEv oxygen ions (current density 0.25 mA cm^{-2}) was accompanied by deposition of the film-forming layer at a rate of about 0.135 μm h^{-1}. As the film became over 0.2 μm thick, the sample was annealed in air at 1173 K for 30 min. The structure thus formed was similar to that of the target; the SiO_2 layer a few tens of nanometres thick simultaneously grown on the silicon substrate acted as the antidiffusion barrier precluding the reaction between the deposits and substrate.

The deposits produced by sputtering of a target with 1.2-kEv argon ions (current density 0.2 mA cm^{-2}) mainly consisted of metallic fractions of the target sputtering products. These layers had low optical transparency and subsequent annealing in air was accompanied by reactions with formation of impurity phases (in particular, orthoferrites near the surface and silicides at the interface with the silicon substrate). Because of this, the formation of the spinel structure is impossible.

Fabrication of oxide film FS structures whose properties are identical to those of bulk ceramics or a single crystal requires that certain problems be solved. First, one should determine the conditions for conformal transfer of the target material to the substrate during the deposition process, as well as to establish optimum conditions for crystallization of the deposited material in the form of a film, because the properties of ferrites with the spinel structure depend strongly on the cation ratio and on mutual cation exchange in the tetrahedral and octahedral sites.[151]

Next, keeping in mind the development of a technology for preparation of film structures on conventional substrates,[152–154] one should avoid (or minimize) the formation of impurity phases at the film/substrate interface due to the chemical reactions between film components and the substrate.

Using various plasma techniques (processing of substrates with microwave oxygen plasma, ion beam sputtering of targets in oxygen or argon atmosphere to grow metal–oxide layers of complex compositions),[147–149] optimum annealing conditions and $Mg(Fe_{0.8}Ga_{0.2})_2O_{4+\delta}$ ceramic targets, spinel films of specified composition on silicon were obtained. $Mg(Fe_{0.8}Ga_{0.2})_2O_{4+\delta}$ is characterized by the specific saturation magnetic moment equal to ~28 A m^2 kg^{-1} (*cf.* ~25 A m^2 kg^{-1} for unsubstituted magnesium ferrite). The bandgap of $Mg(Fe_{0.8}Ga_{0.2})_2O_{4+\delta}$ is 2.4 eV (*cf.* ~2.9 eV for $MgFe_2O_4$).[123] The effect of temperature on the surface structure and morphology on annealing of $Mg(Fe_{0.8+x}Ga_{0.2+y})_2O_{4-\delta}$ spinel films was established.[155]

X-Ray powder diffraction analysis of the films obtained was carried out before and after annealing. $Mg(Fe_{0.8}Ga_{0.2})_2O_{4+\delta}$ ceramic samples had the spinel structure (space group $Fd3m$) with the lattice constant $a = 0.836$ nm and the characteristic reflections at 30.4 (220), 35.6 (113) and 62.8° (400) (see Fig. 15). Films on silicon grown by sputtering of the target with argon ions and subsequent annealing at 1273 K did not have the spinel structure. The major phase was a solid solution based on $GaFeO_3$. The as-produced film grown by sputtering of the target with oxygen ions was amorphous and the X-ray diffraction patterns exhibited only reflections for silicon. Optimization of annealing conditions allowed one to obtain films with the spinel structure. It was found that a temperature of 1073 K is too low to form a homogeneous spinel, although the appearance of the characteristic peak at 35.8° (see Fig. 20 *a*) is noteworthy. Annealing of the films at 1273 K was followed by the appearance of an impurity phase (most likely, hematite α-Fe_2O_3, see Fig. 20 *c*).

By lowering the annealing temperature to 1173 K a spinel film about 200 nm thick was formed. The X-ray diffraction pattern (see Fig. 20 *b*) clearly demonstrates two strong peaks at 30.4 and 35.9° characteristic of the initial ceramic spinel $Mg(Fe_{0.8}Ga_{0.2})_2O_{4+\delta}$.

A layer-by-layer Auger spectroscopy analysis of the sample revealed a considerable deviation from the cation stoichiometry at the film/substrate interface (Fig. 22), which can be explained by a chemical reaction between the film material and the silicon substrate. The thickness of the transient layer in the sample annealed at 1173 K was ~30 nm. After heat treatment, it increased to 60 nm. The impurity phases were not unambiguously identified, but one can assume that they include magnesium, gallium and iron silicates and silicides, as well as silica. The deviation from the initial Mg : Fe : Ga ratio decreased as the films thickness increased, being equal to ~5% only at a depth of 100 nm. Oxygen deficiency was detected throughout the film thickness.

A series of AFM images of these films (Fig. 23) allows one to observe changes in the film surface caused by heat treatment. The sample annealed at 1073 K (Fig. 23 *a*) showed no texturing of the surface and grain boundaries. Its surface is characterized by a plain relief without considerable depth difference (to 2.5 nm) and crystallization effects. The sample annealed at 1173 K (see Fig. 23 *b*) has

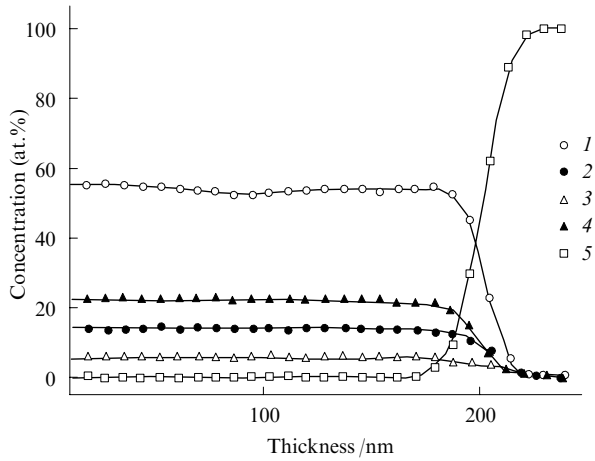


Figure 22. Element distribution profile in the $Mg(Fe_{0.8+x}Ga_{0.2+y})_2O_{4-\delta}$ sample annealed at 1173 K.[155] O (*1*), Mg (*2*), Ga (*3*), Fe (*4*) and Si (*5*).

the crystal structure with regularly cut grains (average grain size is 50 to 100 nm). There are no abrupt depth differences (to 8 nm) and the texture with preferred orientation along the (100) direction is clearly seen. The sample annealed at 1273 K (see Fig. 23 *c*) demonstrates well-defined inclusions of the impurity phase in the form of different-height (to 50 nm) drops of solidified melt, as well as cracks in the film. There are also surface protrusions with a characteristic size of about 1 – 2 μm.

In spite of considerable mismatch of crystallographic parameters and thermal expansion coefficients, spinel-type films of nominal composition $Mg(Fe_{0.8+x}Ga_{0.2+y})_2O_{4-\delta}$ were grown on a silicon substrate. Further studies imply search for a composition to form nanoscale anti-diffusion layers on silicon to suppress the formation of impurity phases at the film/substrate interface and, as a consequence, improvement of the structural and physical properties of the $Mg(Fe_{0.8}Ga_{0.2})_2O_{4+\delta}$ films.

A study [102] which began with a failed attempt to impart an atypical ferromagnetic ordering to the wurtzite structure of ZnO completed with successful isomorphous dissolution of dielectric $MgGa_2O_4$ in the $MgFe_2O_4$ magnetic matrix using the concept of the 'reverse' spinel structure. Then, an entire process flow from polycrystalline powder to ceramics and then to a film was reproduced on the laboratory scale.[155]

The proposed method for the preparation of oxide FS materials is of limited use. As the percolation threshold is reached (33% of Fe^{3+} cations are replaced by Ga^{3+}), the long-range magnetic order is destroyed, the ferromagnetic spinel structure becomes strongly frustrated and local distortions are formed, *i.e.*, the material loses its homogeneity and clustering becomes feasible.[156]

* * *

A decade of research using the DMS approach [8, 157] did not lead to preparation of a material whose FS properties are better than those of (Ga,Mn)As with T_C = 190 K.[157] Meanwhile, the authors of early studies [158] assumed the presence of clusters based on ferromagnetic manganese arsenides MnAs (T_C = 318 K) and Mn_2As (T_C = 580 K) in the GaAs matrix. Similarly to the case where a limited amount of manganese dissolves in GaAs, a limited amount of gallium dissolves in the phases based on manganese arsenides. Correspondingly, replacement of a magnetic cation by nonmagnetic one causes a decrease in T_C of (Mn,Ga)As or $(Mn,Ga)_2As$ clusters present in the GaAs matrix.

Taking oxides as an example, in this review we have shown the feasibility of fabricating multilayer ferromagnet – semiconductor composite films and monolayer homogeneous FS films. However, unlike ceramics, preparation of

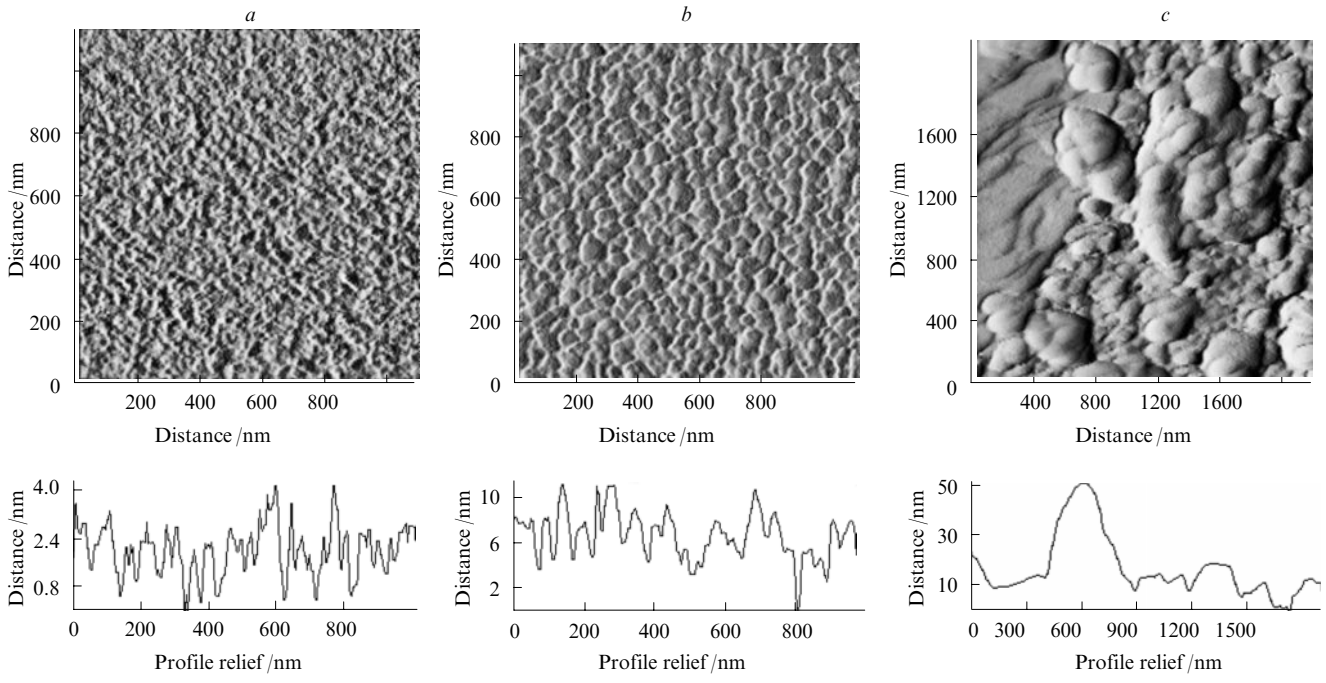


Figure 23. AFM images of the surface morphology of $Mg(Fe_{0.8+x}Ga_{0.2+y})_2O_{4-\delta}$ films annealed at 1073 (*a*), 1173 (*b*) and 1273 K (*c*).[155]

such materials is a very labour-consuming process which requires continuous control of all steps. Unstable reproducibility makes large-scale (industrial) use of these methods impossible.

Being very attractive, the DMS approach still remains of academic interest only. However, there is also a research avenue for further search for spintronics materials, *viz*., multicomponent oxide FS compounds. Probably, they will be found among the Aurivillius phases[159] or complex perovskites.[160]

References

1. B T Matthias, R M Bozorth, J H van Vleck *Phys. Rev. Lett*. **7** 160 (1961)
2. A S Borukhovich *Fizika Materialov i Struktur Sverkhprovodyashchei i Poluprovodnikovoi Spinovoi Elektroniki* (The Physics of Materials and Structures of Superconducting and Semiconductor Spin Electronics) (Ekaterinburg: Ural Branch of the Russian Academy of Sciences, 2004)
3. E L Nagaev *Fizika Magnitnykh Poluprovodnikov* (The Physics of Magnetic Semiconductors) (Moscow: Nauka, 1979)
4. L I Koroleva *Magnitnye Poluprovodniki* (Magnetic Semiconductors) (Moscow: Moscow State University, 2003)
5. X Wan, J Dong, S Y Savrasov *Phys. Rev. B: Condens. Matter* **83** 205201 (2011)
6. V G Bamburov, A S Borukhovich, A A Samokhvalov *Vvedenie v Fiziko-khimiyu Ferromagnitnykh Poluprovodnikov* (Introduction in Physical Chemistry of Ferromagnetic Semiconductors) (Moscow: Metallurgiya, 1988)
7. H Ohno, A Shen, F Matsukura, A Oiwa, A Endo, S Katsumoto, Y Iye *Appl. Phys. Lett*. **69** 363 (1996)
8. T Dietl, H Ohno, F Matsukura, J Cibert, D Ferrand *Science* **87** 1019 (2000)
9. K Sato, H Katayama-Yoshida *Jpn. J. Appl. Phys*. **40** 334 – 336 (2001)
10. C Liu, F Yun, H Morkoç *J. Mater. Sci., Mater. Electron*. **16** 555 (2005)
11. Ü Özgür, Ya I Alivov, C Liu, A Teke, M A Reshchikov, S Doğan, V Avrutin, S-J Cho, H Morkoç *J. Appl. Phys*. **98** 103 (2005)
12. R Seshadri *Curr. Opin. Solid State Mater. Sci*. **9** 1 (2005)
13. T Fukumura, H Toyosaki, Y Yamada *Semicond. Sci. Technol*. **20** S103 (2005)
14. I Djerdj, Z Jagličić, D Arčon, M Niederberger *Nanoscale* **2** 1096 (2010)
15. A Ney *Materials* **3** 3565 (2010)
16. C Song, K W Geng, F Zeng, X B Wang, Y X Shen, F Pan, Y N Xie, T Liu, H T Zhou, Z Fan *Phys. Rev. B: Condens. Matter* **73** 024405 (2006)
17. S Krishnamurthy, C McGuinness, L S Dorneles, M Venkatesan, J M D Coey, J G Lunney, C H Patterson, K E Smith, T Learmonth, P-A Glans *J. Appl. Phys*. **99** 08M111 (2006)
18. A Fouchet, W Prellier, B J Mercey *J. Appl. Phys*. **100** 013901 (2006)
19. Y B Zhang, S Li, G K L Goh, S Tripathy *Appl. Phys. Lett*. **93** 102510 (2008)
20. Q Xu, L Hartmann, S Zhou, A Mcklich, M Helm, G Biehne, H Hochmuth, M Lorenz, M Grundmann, H Schmidt *Phys. Rev. Lett*. **101** 076601 (2008)
21. Z Yang, M Biasini, W P Beyermann, M B Katz, O E Ezekoye, X Q Pan, Y Pu, J Shi, Z Zuo, J L Liu *J. Appl. Phys*. **104** 113712 (2008)
22. N Akdoğan, B Rameev, S Güler, O Öztürk, B Aktas, H Zabel, R Khaibullin, L Tagirov *Appl. Phys. Lett*. **95** 102502 (2009)
23. Y B Zhang, S Li, G K L Goh *J. Appl. Phys*. **105** 07C504 (2009)
24. N Akdogan, H Zabel, A Nefedov, K Westerholt, H-W Becker, S Glk, R Khaibullin, L Tagirov *J. Appl. Phys*. **105** 043907 (2009)
25. J Ji, A Zhang, T Xia, Q Cao, G Liu, D Hou, Q Zhang *Phys. Rev. B: Condens. Matter* **82** 014408 (2010)
26. S Han, D Zhang, C Zhou *Appl. Phys. Lett*. **88** 133109 (2006)
27. J Cui, Q Zeng, U J Gibson *J. Appl. Phys*. **99** 08M113 (2006)
28. J Cui, U Gibson *Phys. Rev. B: Condens. Matter* **74** 045416 (2006)
29. J W Chiou, H M Tsai, C W Pao, K P Krishna Kumar, J H Chen, D C Ling, F Z Chien, W F Pong, M-H Tsai, J J Wu *Appl. Phys. Lett*. **90** 062103 (2007)
30. C Y Lin, W H Wang, C-S Lee, K W Sun, Y W Suen *Appl. Phys. Lett*. **94** 151909 (2009)
31. S Maensiri, P Laokul, J Klinkaewnarong, C Thomas *Appl. Phys. A* **94** 601 (2009)
32. B-B Li, H-L Shen, R Zhang, X-Q Xiu, Z Xie *Chin. Phys. Lett*. **24** 3473 (2007)
33. K R Kittilstved, D R Gamelin *J. Appl. Phys*. **99** 08M112 (2006)
34. H Matsui, H Tabata *Phys. Rev. B: Condens. Matter* **75** 014438 (2007)
35. M Ivil, S J Pearton, S Rawal, L Leu, P Sadik, R Das, A F Hebard, M Chisholm, J D Budai, D P Norton *New J. Phys*. **10** 065002 (2008)
36. S Ghoshal, P S Anil Kumar *J. Phys. B: Condens. Matter* **20** 192201 (2008)
37. T C Kaspar, T Droubay, S M Heald, M H Engelhard, P Nachimuthu, S A Chambers *Phys. Rev. B, Condens. Matter* **77** 201303 (2008)
38. S M Heald, T C Kaspar, T Droubay, V Shutthanandan, S A Chambers, A Mokhtari, A J Behan, H J Blythe, J R Neal, M Fox, G Gehring *Phys. Rev. B: Condens. Matter* **79** 075202 (2009)
39. Z Y Wu, F R Chen, J J Kai, W B Jian, J J Lin *Nanotechnology* **17** 5511 (2006)
40. V K Sharma, G D Varma *Cryst. Res. Technol*. **43** 1046 (2008)
41. Y Lee, J C Lee, C-W Su *IEEE Trans. Magn*. **46** 1565 (2010)
42. J Blasco, F Bartolomé, L M García, J García *J. Mater. Chem*. **16** 2282 (2006)
43. M Opel, K-W Nielsen, S Bauer, S T B Goennenwein, J C Cezar, D Schmeisser, J Simon, W Mader, R Gross *Eur. Phys. J. B* **63** 437 (2008)
44. M Tay, Y H Wu, G C Han, Y B Chen, X Q Pan, S J Wang, P Yang, Y P Feng *J. Mater. Sci.: Mater. Electron*. **20** 60 (2009)
45. W Jian, Z Wu, R Huang, F Chen, J Kai, C Wu, S Chiang, M Lan, J Lin, *Phys. Rev. B: Condens. Matter* **73** 233308 (2006)
46. Y Zhang, T Sritharan, S Li *Phys. Rev. B: Condens. Matter* **73** 172404 (2006)
47. M S Moreno, T Kasama, R E Dunin-Borkowski, D Cooper, P A Midgley, L B Steren, S Duhalde, M F Vignolo *J. Phys. D: Appl. Phys*. **39** 1739 (2006)
48. X-C Liu, E-W Shi, Z-Z Chen, H-W Zhang, T Zhang, L-X Song *Chinese Phys*. **16** 1770 (2007)
49. T C Kaspar, T Droubay, S M Heald, P Nachimuthu, C M Wang, V Shutthanandan, C A Johnson, D R Gamelin, S A Chambers *New J. Phys*. **10** 055010 (2008)
50. Ney, K Ollefs, S Ye, T Kammermeier, V Ney, T C Kaspar, S A Chambers, F Wilhelm, A Rogalev *Phys. Rev. Lett*. **100** 157201 (2008)
51. T Kammermeier, V Ney, S Ye, K Ollefs, T C Kaspar, S A Chambers, F Wilhelm, A Rogalev, A Ney *J. Magn. Magn. Mater*. **321** 699 (2009)
52. A Ney, T Kammermeier, K Ollefs, S Ye, V Ney, T C Kaspar, S A Chambers, F Wilhelm, A Rogalev *Phys. Rev. B: Condensed Matter* **81** 054420 (2010)
53. B Witkowski, M Godlewski, E Guziewicz, M Sawicki, W Paszkowicz, R Jakieła, T A Krajewski, G Łuka, M I Łukasiewicz *Phys. Status Solidi B* **247** 1666 (2010)

54. T C Kaspar, T Droubay, D E McCready, P Nachimuthu, S M Heald, C M Wang, A S Lea, V Shutthanandan, S A Chambers, M F Toney *J. Vacuum Sci. Technol., B* **24** 2012 (2006)
55. H-Q Song, L-M Mei, S-S Yan, X-L Ma, J-P Liu, Y Wang, Z Zhang *J. Appl. Phys.* **99** 123903 (2006)
56. H-Q Song, Y Wang, S-S Yan, L-M Mei, Z Zhang *J. Magn. Magn. Mater.* **312** 53 (2007)
57. R Ramaneti, J C Lodder, R Jansen *Appl. Phys. Lett.* **91** 012502 (2007)
58. A F Orlov, L A Balagurov, I V Kulemanov, N S Perov, E A Gan'shina, L Yu Fetisov, A Rogalev, A Smekhova, J C Cezar *Fiz. Tv. Tela* **53** 452 (2011) [a]
59. B Z Jiang, T L Phan, D S Yang, K W Lee, S C Yu *Solid State Commun.* **150** 1932 (2010)
60. B Choudhury, A Choudhury, A K M Maidul Islam, P Alagarsamy, M Mukherjee, *J. Magn. Magn. Mater.* **323** 440 (2011)
61. K Ando *Science*. **312** 1883 (2006)
62. A Fert *Rev. Mod. Phys.* **80** 1517 (2008)
63. N A Toropov, V P Barzakovskii, I A Bodnar', Yu P Udalov, in *Diagrammy Sostoyaniya Silikatnykh Sistem. Spravochnik. Metall-kislorodnye Soedineniya Silikatnykh Sistem* (Equilibrium Diagrams of Silicate Systems. Handbook. Metal – Oxygen Compounds of Silicate Systems) (Leningrad: Nauka, 1969) No. 2 p. 372
64. E K Kazenas, Yu V Tsvetkov *Isparenie Oksidov* (Evaporation of Oxides) (Moscow: Nauka, 1997)
65. Y Matsumoto, M Murakami, T Shono, T Hasegawa, T Fukumura, M Kawasaki, P Ahmet, T Chikyow, S-Y Koshihara, H Koinuma *Science* **291** 854 (2001)
66. I-B Shim, S-Y An, C S Kim, S-Y Choi, Y W Park *J. Appl. Phys.* **91** 7914 (2002)
67. N H Hong, J Sakai, W Prellier, A Hassini *Appl. Phys. Lett.* **83** 3129 (2003)
68. N H Hong, W Prellier, J Sakai, A Ruyter *J. Appl. Phys.* **95** 7378 (2004)
69. S A Chambers, S Thevuthasan, R F C Farrow, R F Marks, J U Thiele, L Folks, M G Samant, A J Kellock, N Ruzycki, D L Ederer, U Diebold *Appl. Phys. Lett.* **79** 3467 (2001)
70. M Murakami, Y Matsumoto, T Hasegawa, P Ahmet, K Nakajima, T Chikyow, H Ofuchi, I Nakaiand, H Koinuma *J. Appl. Phys.* **95** 5330 (2004)
71. W K Park, R J Ortega-Hertogs, J S Moodera, A Punnoose, M S Seehra *J. Appl.Phys.* **91** 8093 (2002)
72. V Shutthanandan, S Thevudasan, S M Heald, T Droublay, M H Englehard, T C Kasper, D E McCready, L Saraf, S A Chambers, B S Mun, N M Hamdan, P Nachimuthu, B Taylor, R P Searsand, B Sinkovic *Appl. Phys. Lett.* **84** 4466 (2004)
73. R Suryanarayanan, V M Naik, P Kharel, P Talgala, R Naik *Solid State Commun.* **133** 439 (2005)
74. A I Stognij, M V Pashkevich, N N Novitskii, A V Bespalov *Pis'ma Zh. Tekh. Fiz.* **36** 73 (2010) [b]
75. Yu A Dynnik, I S Edel'man, T P Morozova, P D Kim, I A Turpanov, A Ya Beten'kova *Pis'ma Zh. Eksp. Teor. Fiz.* **65** 531 (1997) [c]
76. L V Lutsev, A I Stognij, N N Novitskii *Pis'ma Zh. Eksp. Teor. Fiz.* **81** 636 (2005) [c]
77. A I Stognij, V F Meshcheryakov, N N Novitskii, F Fettar, M V Pashkevich *Pis'ma Zh. Tekh. Fiz.* **35** 97 (2009) [b]
78. A I Stognij, M V Pashkevich, N N Novitskii, A V Bespalov, V A Ketsko, F Fettar, H Garad *Neorg. Mater.* **45** 1323 (2009) [d]
79. A I Stognij, N N Novitskii, O M Stukalov *Pis'ma Zh. Tekh. Fiz.* **28** 39 (2002) [b]
80. A I Stognij, N N Novitskii, O M Stukalov *Pis'ma Zh. Tekh. Fiz.* **29** 39 (2003) [c]
81. T M R Viseu, B Almeida, M Stchakovsky, B Drevillon, M I C Ferreira, J B Sousa *Thin Solid Films* **401** 216 (2001)
82. L Feldman, D Mayer *Fundamentals of Surface and Thin Film Analysis* (New York: North Holland, 1986)
83. L Sangaletti, F F Canova, A Sepe, S Pagliara, M C Mozzati, P Galinetto, C B Azzoni, A Speghini, M Bettinelli *Surf. Sci.* **601** 4375 (2007)
84. T Trypiniotis, D H Y Tse, S J Steinmuller, W S Cho, J A C Bland *IEEE Trans. Magn.* **43** 2872 (2007)
85. Z Jin, T Fukumura, M Kawasaki, K Ando, H Saito, T Sekiguchi, Y Z Yoo, M Murakami, Y Matsumoto, T Hasegawa, H Koinuma *Appl. Phys. Lett.* **78** 3824 (2001)
86. K Ueda, H Tabata, T Kawa *Appl. Phys. Lett.* **79** 988 (2001)
87. V K Sharma, R Xalxo, G D Varma *Cryst. Res. Technol.* **42** 34 (2007)
88. H-J Lee, S-E Jeong, C R Cho, C H Park *Appl. Phys. Lett.* **81** 4020 (2002)
89. S G Yang, A B Pakhomov, S T Hung, C Y Wong *IEEE Trans. Magn.* **38** (5) 2877 (2002)
90. S-W Lim , D-K Hwang, J-M Myoung *Solid State Commun.* **125** 231 (2003)
91. S Ramachandran, A Tiwari, J Narayan *Appl. Phys. Lett.* **84** 5255 (2004)
92. J H Kim, H Kim, D Kim, Y E Ihm, W K Choo *J. Appl. Phys.* **92** 6066 (2002)
93. G Lawes, A S Risbud, A P Ramirez, Ram Seshadri *Phys. Rev. B: Condens. Matter* **71** 1 (2005)
94. M H Kane, K Shalini, C J Summers, R Varatharajan, J Nause, C R Vestal, Z J Zhang, I T Ferguson *J. Appl. Phys.* **97** 023906 (2005)
95. K Rode, A Anane, R Mattana, J-P Contour, O Durand, R LeBourgeois *J. Appl. Phys.* **93** 7676 (2003)
96. A Navrotsky, A Muan *J. Inorg. Nucl. Chem.* **32** 3471 (1970)
97. A Navrotsky, A Muan *J. Inorg. Nucl. Chem.* **33** 35 (1971)
98. B Ficher, D S Tannhauser *J. Electrochem. Soc.* **111** 1194 (1964)
99. V B Lazarev, V V Sobolev, I S Shaplygin *Khimicheskie i Fizicheskie Svoistva Prostykh Oksidov Metallov* (Chemical and Physical Properties of Simple Metal Oxides) (Moscow: Nauka, 1983)
100. Yu V Levinskii *p – T – x-Diagrammy Sostoyaniya Dvoinykh Metallicheskikh Sistem (Spravochnik)* [*p – T – x*-Equilibrium Diagrams of Binary Metal Systems (Handbook)] (Moscow: Metallurgiya, 1990) Vol. 1
101. N P Lyakishev, O A Bannykh, L L Rokhlin, S P Alisova, N R Bochvar, P B Budberg, T V Dobatkina, B V Lysova, V P Polyakova, K B Povarova, M L Tylkina, L B Shelimova, B N Sheftel' *Diagrammy Sostoyaniya Dvoinykh Metallicheskikh Sistem. (Spravochnik)* [Equilibrium Diagrams of Double Metal Systems (Handbook)] (Moscow: Mashinostroenie, 1997) Vol. 2
102. G D Nipan, V A Ketsko, T N Kol'tsova, A I Stognij, K I Yanushkevich, V V Pan'kov, A M Khoviv, A M Solodukha *Zh. Neorg. Khim.* **51** 2083 (2006) [e]
103. K S Gavrichev, A V Tyurin, M A Ryumin, A V Khoroshilov, G D Nipan, V A Ketsko, T N Kol'tsova, I Yu Pinus, G A Buzanov, N A Votinova *Zh. Neorg. Khim.* **54** 3 (2009) [e]
104. H J Kim, I C Song, J H Sim, H Kim, D Kim, Y E Ihm, W K Choo *J. Appl. Phys.* **95** 7387 (2004)
105. G D Nipan, V A Ketsko, A I Stognij, N T Kuznetsov *Inorg. Mater.* **46** 1437 (2010) [d]
106. A Quesada, M A García, M Andrés, A Hernando, J F Fernández, A C Caballero, M S Martín-González, F Briones *J. Appl. Phys.* **100** 113909 (2006)
107. G D Nipan, Ya Kh Grinberg, V B Lazarev in *Termodinamika i Materialovedenie Poluprovodnikov* (Thermodynamics and Materials Sciences of Semiconductors) (Ed. V M Glazov) (Moscow: Metallurgiya, 1992) p. 392
108. B P Zakharchenya, V L Korenev *Usp. Fiz. Nauk* **175** 630 (2005) [f]
109. A R West *Solid State Chemistry and its Applications* (Chichester: Wiley, 1984)

110. Yu D Tretyakov, N N Oleinikov, V A Granik, in *Fiziko-khimicheskie Osnovy Termicheskoi Obrabotki Ferritov* (Physicochemical Foundation of Ferrite Thermal Treatment) (Moscow: Moscow State University, 1977) p. 202
111. V B Lazarev, V G Krasov, I S Shaplygin, in *Elektroprovodnost' Oksidnykh Sistem i Plenochnykh Struktur* (Conductivity of Oxide Systems and Film Structures) (Moscow: Nauka, 1978) p. 168
112. D Venkatesshvaran, M Althammer, A Nielsen, S Geprigs, M S Ramachandra Rao, S T B Goennenwien, M Opel, R Gross *Phys. Rew. B: Condens. Matter* **79** 134405 (2009)
113. A S Risbud, R Seshadri, J Ensling, C Felser *J. Phys.: Condens. Matter* **17** 1003 (2005)
114. G S Mattioli, B J Wood, I S E Carmichael *Am. Mineral.* **72** 468 (1987)
115. J Nell, B J Wood, T O Mason *Am. Mineral.* **74** 339 (1989)
116. J Nell, B J Wood *Am. Mineral.* **74** 1000 (1989)
117. R J Harrison, A Putnis *Am. Mineral.* **80** 213 (1995)
118. R J Harrison, A Putnis *Am. Mineral.* **81** 375 (1996)
119. R J Harrison, M T Dove, K S Knight, A Putnis *Am. Mineral.* **84** 555 (1999)
120. M Gateshki, V Petkov, S K Pradhan, T Vogt *J. Appl. Crystallogr.* **38** 772 (2005)
121. L M Letyuk, in *Kristallokhimicheskie Problemy Materialovedeniya Poluprovodnikov* (Crystal Chemical Problems of Materials Science of Semiconductors) (Moscow: Nauka, 1975) p. 136
122. K B Modi, H H Joshi, R G Kulkarni *J. Mater. Sci.* **31** 1311 (1996)
123. G D Nipan, V A Ketsko, A I Stognij, A V Trukhanov, T N Kol'tsova, E N Beresnev, M A Kop'eva, L V Elesina, N T Kuznetsov *Dokl. Akad. Nauk* **430** 783 (2010) [g]
124. G D Nipan, V A Ketsko, A I Stognij, A V Trukhanov, T N Kol'tsova, E N Beresnev, M A Kop'eva, L V Elesina, N T Kuznetsov *Neorg. Mater.* **46** 490 (2010) [d]
125. A S Mukasyan, P Dinka *Int. J. Self-Propag. High-Temp. Synth.* **16** 23 (2007)
126. V A Ketsko, E N Beresnev, M A Kop'eva, L V Ryabkova, A E Baranchikov, A I Stognij, A V Trukhanov, N T Kuznetsov *Zh. Neorg. Khim.* **55** 476 (2010) [e]
127. J-C Tellier *Rev. Chim. Miner.* **4** 325 (1967)
128. B I Pokrovskii, A K Gapeev, A N Goryaga, L N Komissarova, in *Ferrimagnetizm* (Ferrimagnetism) (Moscow: Moscow State University, 1975) p. 208
129. C O Arean, J L R Blanco, M C T Fernandez *J. Chem. Soc., Faraday Trans.* **88** 321 (1992)
130. G D Nipan, V A Ketsko, T N Kol'tsova, M A Kop'eva, A I Stognij, A V Trukhanov *Neorg. Mater.* **46** 1134 (2010) [d]
131. L S Darken, R W Gurry *J. Am. Chem. Soc.* **68** 798 (1946)
132. Yu D Tretyakov, in *Termodinamika Ferritov* (Thermodynamics of Ferrites) (Leningrad: Khimiya, 1967) p. 304
133. D Woodhouse, J White *Trans. Brit. Ceram. Soc.* **54** 333 (1955)
134. A E Paladino *J. Am. Ceram. Soc.* **43** 183 (1960)
135. H J Van Hook *J. Am. Ceram. Soc.* 470 (1965)
136. J Ghose *J. Solid State Chem.* **79** 189 (1989)
137. M Zinkevich, S Geupel, F Aldinger *J. Alloys Compd.* **393** 154 (2005)
138. A S Berezhnoi, in *Mnogokomponentnye Sistemy Okislov* (Multicomponent Systems of Oxides) (Kiev: Naukova Dumka, 1970) p. 544
139. N A Toropov, V P Barzakovskii, V V Lapin, N N Kurtseva, in *Diagrammy Sostoyaniya Silikatnykh Sistem (Spravochnik)* [Equilibrium Diagrams of Silicate Systems (Handbook)] (Leningrad: Nauka, 1969) No. 1, p. 822
140. B L Phillips, S Somiya, A Muan *J. Am. Ceram. Soc.* **44** 167 (1961)
141. A N Men', Yu P Vorob'ev, G I Chufarov, in *Fiziko-khimicheskie Svoistva Nestekhiometricheskikh Okislov* (Physicochemical Properties of Nonstoichiometric Oxides) (Leningrad: Khimiya, 1973) p. 224
142. B Malaman, H Alebouyeh, F Jeannot, A Courtois, R Gérardin, O Evrard *Mater. Res. Bull.* **16** 1139 (1981)
143. W Kwestroo *J. Inorg. Nucl. Chem.* **9** 65 (1959)
144. L M Letyuk, N V Troneva *Neorg. Mater.* **9** 1596 (1973) [d]
145. A Navrotsky, O Kleppa *J. Inorg. Nucl. Chem.* **29** 2701 (1967)
146. V V Pan'kov, A I Stognij, V D Koshevar, V A Ketsko *Neorg. Mater.* **44** 1144 (2008) [d]
147. A P Ges', A V Zubets, A I Stognij, V V Tokarev, V V Fedotova *Pis'ma Zh. Tekn. Fiz.* **16** 65 (1990) [b]
148. A I Stognij, S V Koryakin, A V Marchenko, A I Demchenko, V I Khit'ko *Pribor. Tekhn. Eksp.* (4) 164 (2004) [h]
149. A I Stognij, N N Novitskii, S D Tushina, S V Kalinnikov *Zh. Tekh. Fiz.* **73** 86 (2003) [i]
150. A I Stognij, A V Trukhanov, V A Ketsko, G D Nipan *Neorg. Mater.* **47** 247 (2011) [d]
151. E W Gorter *Phil. Res. Rep.* **9** 295 (1954)
152. L V Lutsev, A I Stognij, N N Novitskii, A A Stashkevich *J. Magn. Magn. Mater.* **300** 12 (2006)
153. T V Murzina, A V Shebarshin, I A Kolmychek, E A Gan'shina, O A Aktsipetrov, A I Stognij, N N Novitskii, A Stashkevich *Zh. Eksp. Teor. Fiz.* **136** 123 (2009) [j]
154. L V Lutsev, A I Stognij, N N Novitskij *Phys. Rev.* **80** 184423 (2009)
155. A V Trukhanov, A I Stognij, N N Novitskii, S V Trukhanov, V A Ketsko *Neorg. Mater.* **47** 1128 (2011) [d]
156. J Hubsch, G Gavoille, J Bolfa *J. Appl. Phys.* **49** 1363 (1978)
157. T Dietl *Nat. Mater.* **9** 965 (2010)
158. K S Zhuravlev, T S Shamirzaev, N A Yakusheva *Fiz. Tekh. Poluprovod.* **32** 791 (1998) [k]
159. Srinivas, T Sritharan, F Y C Boey *J. Appl. Phys.* **98** 036104 (2005)
160. T Yang, T Perkisas, J Hadermann, M Croft, A Ignatov, G Van Tendaloo, M Greenblatt *J. Mater. Chem.* **21** 199 (2011)

[a] — *Phys. Solid State (Engl. Transl)*
[b] — *J. Tech. Phys. Lett. (Engl. Transl.)*
[c] — *J. Exp. Theor. Phys. Lett. (Engl. Transl.)*
[d] — *Inorg. Mater. (Engl. Transl.)*
[e] — *Russ. J. Inorg. Chem. (Engl. Transl.)*
[f] — *Physics-Uspekhi (Engl. Transl.)*
[g] — *Dokl. Phys. (Engl. Transl.)*
[h] — *Instrum. Exp. Tech. (Engl. Transl.)*
[i] — *J. Tech. Phys. (Engl. Transl.)*
[j] — *J. Exp. Theor. Phys. (Engl. Transl.)*
[k] — *Semiconductors (Engl. Transl.)*